Available online at www.sciencedirect.com
ScienceDirect
Precambrian Research 161 (2008) 279–302
Precambrian Research
www.elsevier.com/locate/precamres

Zircon geochronology of granitoids from the western Bacajá domain, southeastern Amazonian craton, Brazil: Neoarchean to Orosirian evolution

Marcelo L. Vasquez [a,b,*], Moacir J.B. Macambira [b], Richard A. Armstrong [c]

[a] *Geological Survey of Brazil, CPRM, Belém, PA, Brazil*
[b] *Isotope Geology Laboratory, Federal University of Pará, CxP 8608, CEP 66075-110, Belém, Pará, Brazil*
[c] *Research School of Earth Science, Australian National University, Canberra, ACT 0200, Australia*

Received 27 October 2006; received in revised form 1 September 2007; accepted 3 September 2007

Abstract

New zircon U–Pb SHRIMP and Pb-evaporation data on rocks from the west part of the Bacajá domain, southeastern Amazonian craton, reveal crustal evolution marked by a succession of magmatic events from Neoarchean to Orosirian. This domain represents the southern part of a geochronological province of the Amazonian craton that evolved during the Trans-Amazonian cycle (2.26–2.0 Ga).

The earliest event is represented by inliers of ca. 2.67, 2.5 and 2.45 Ga orthogneisses and supracrustal rocks, followed by the formation of a 2.36–2.34 Ga granitoid-greenstone terrane and 2.31 Ga granitoids. Rhyacian granitoids and charnockitic rocks marked the main evolutionary stages of the Bacajá domain. Rhyacian magmatic events were distinguished in this domain: 2.21, 2.18, 2.16–2.15 and 2.13 Ga granitoids related to magmatic arcs of the Trans-Amazonian orogenies; 2.10–2.09 and 2.08–2.07 Ga granitoids and charnockitic rocks related to the post-collisional stage. A younger magmatic event at 1.99 Ga remains controversial, as it is uncertain whether this represents the last magmatic pulse of the Trans-Amazonian cycle or whether it is related to a younger cycle which affected the adjacent domain.

Although Archean rock remnants have been found in Trans-Amazonian domains from South America, Siderian rocks are rare and distinguish the Bacajá domain from other Trans-Amazonian orogens of the Amazonian craton.

Keywords: Zircon geochronology; Amazonian craton; Trans-Amazonian cycle; Granitoids; Orthogneisses

1. Introduction

The Bacajá domain is located in the southeastern part of the Amazonian craton and represents the southern part of the Maroni-Itacaiúnas province (Cordani et al., 1979; Tassinari and Macambira, 1999, 2004), or Trans-Amazonian province (Santos, 2003). Previous isotope data indicated that the rocks from this domain are related to the Trans-Amazonian cycle and age constraints were first proposed in the 1980s, mainly based on Rb–Sr and K–Ar data (referred in Cordani et al., 1984). The Rb–Sr data suggested Paleoproterozoic reworking of the gneisses of the basement and the addition of a juvenile mafic volcanic crust (Cordani et al., 1984; Santos et al., 1988; Teixeira et al., 1989) that distinguished it from the Archean Central Amazonian province to the south. The first zircon Pb-evaporation, Nd isotopes and U–Pb SHRIMP data confirmed the formation of Rhyacian rocks (2.21–2.08 Ga) and local occurrences of Neoarchean (2.67 Ga), early Siderian (2.50–2.44 Ga), late Siderian (2.36–2.31 Ga) and Orosirian (1.99 Ga) rocks (Macambira et al., 2001, 2003, 2004; Santos, 2003; Faraco et al., 2005; Vasquez et al., 2005).

Paleoproterozoic rocks are extensively represented in the Precambrian of South America, especially during the Trans-Amazonian cycle when the continental crust experienced most important period of growth (Cordani and Sato, 1999; Schobbenhaus and Brito Neves, 2003). The Trans-Amazonian is present in the southern part of South America, in the São Francisco, São Luís and Amazonian cratons and may be correlated with orogenies in the West African and Congo cratons (Bertrand and Jardim de Sá, 1990; Ledru et al., 1994; Tassinari and Macambira, 1999; Santos et al., 2003a). Although

* Corresponding author at: Companhia de Pesquisa de Recursos Minerais, Av. Dr. Freitas, 3645, CEP 66095-110, Belém, Pará, Brazil. Tel.: +55 91 3182 1326; fax: +55 91 32764020.
E-mail addresses: vasquez@be.cprm.gov.br (M.L. Vasquez), moamac@ufpa.br (M.J.B. Macambira), Richard.Armstrong@anu.edu.au (R.A. Armstrong).

0301-9268/$ – see front matter © 2007 Elsevier B.V. All rights reserved.
doi:10.1016/j.precamres.2007.09.001

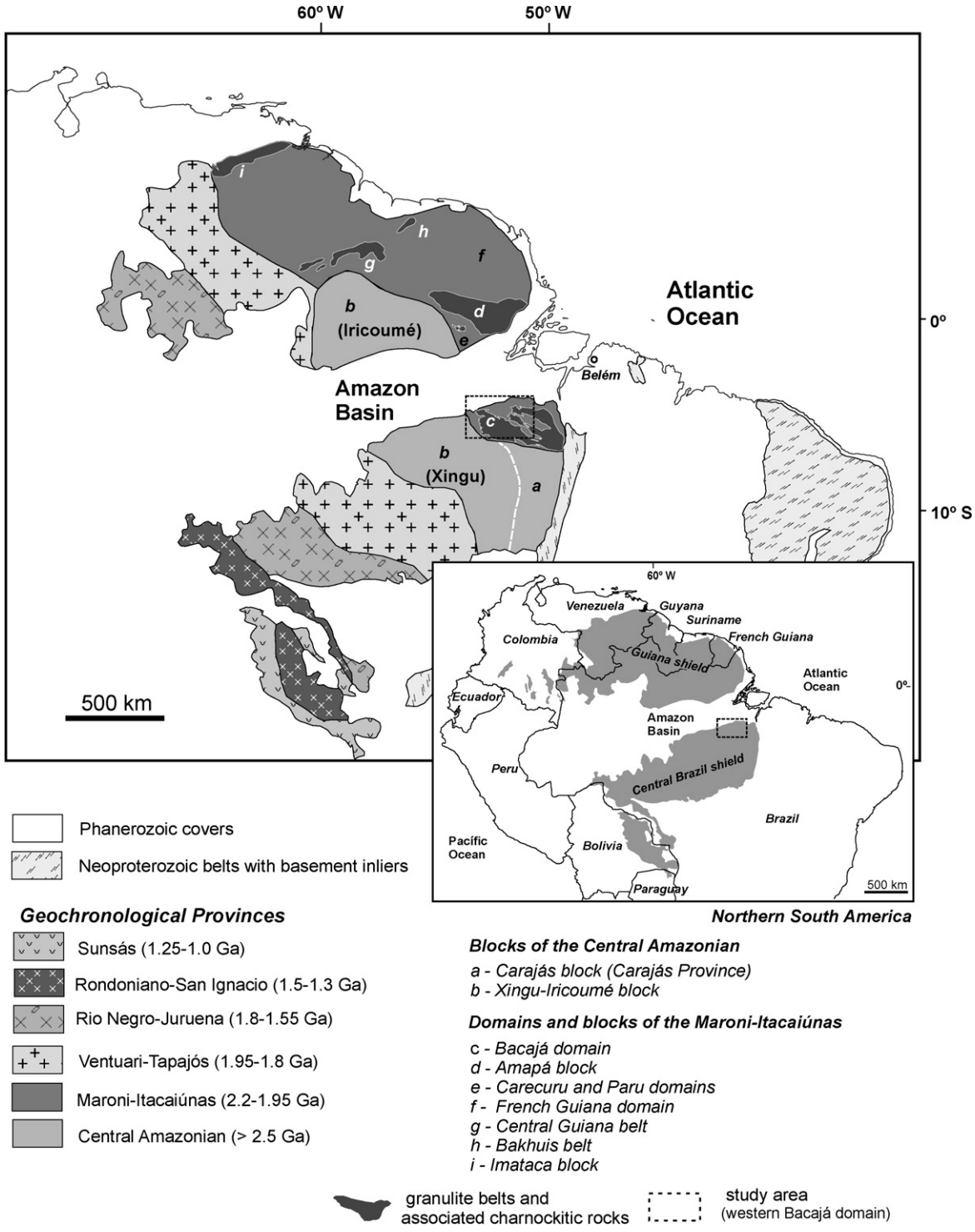

Fig. 1. Sketch maps of the Amazonian craton with the location of the study area, the geochronological provinces based on Tassinari and Macambira (2004) and the different segments of the Central Amazonian and Maroni-Itacaiúnas provinces.

reworking of Archean crust was common during the Trans-Amazonian cycle, the formation of juvenile crust was important during these orogenies, especially in the Amazonian craton (Cordani and Sato, 1999; Tassinari and Macambira, 1999). Studies in the domains of the Maroni-Itacaiúnas province have shown they have peculiarities that distinguish them in spite of the Trans-Amazonian geological evolution. For example, in French Guiana (Fig. 1) there is a predominance of juvenile rocks (Vanderhaeghe et al., 1998; Delor et al., 2003a), whereas the Archean component is extensive in the Amapá block (Avelar et al., 2003; Rosa-Costa et al., 2006).

The Bacajá domain is the closest Trans-Amazonian domain to the main Archean domain of the Amazonian craton, the Carajás block or province (Fig. 1), and is therefore a key area to the under-

Table 1
Summary of the previous geochronological data of rocks from the Bacajá domain

Period[a]	Unit	Area	Rock	Pb-evaporation on zircon (Ma)	U–Pb SHRIMP on zircon (Ma)	Sm–Nd (WR) T_{DM} (Ga)/εNd_t	Ref.
Neoarchean (2850–2500 Ma)	Orthogneisses	Manelão	Tonalitic gneiss	2671 ± 3		2.67/+2.66	(1)
		Uruará			2503 ± 10/2581 ± 6[b]		(2)
		Brasil Novo	Tonalitic gneiss	2440 ± 7			(3)
Siderian (2500–2300 Ma)	Metasedimentary rocks of high-grade	Uruará	Garnet-biotite gneiss (pelitic gneiss)	2361–2076			(3)
	Supracrustal rocks	Três Palmeiras	Metandesite	2359 ± 3			(1)
Rhyacian (2300–2050 Ma)	Granitoids	Novo Repartimento	Metatonalite		2313 ± 9		(4)
		Brasil Novo	Granodiorite	2215 ± 2			(3)
		Brasil Novo	Tonalite		2182 ± 6		(2)
		Belo Monte	Granodiorite	2154 ± 2		2.35/+0.21	(5)
		Novo Repartimento	Granodiorite		2114 + 35/−33		(4)
		Uruará	Monzogranite	2104 ± 5			(3)
		Brasil Novo	Monzogranite	2077 ± 2			(3)
		Novo Repartimento	Granodiorite	2076 ± 6			(6)
		Novo Repartimento	Granodiorite	2075 ± 3		2.57/−4.12 and 2.25–2.35/+0.83 to −0.60	(5)
		Manelão	Monzogranite	2069 ± 6			(7)
	Charnockitic rocks	Volta Grande	Charnockite		2086 ± 5		(2)
Orosirian (2050–1800 Ma)	Granitoids	Uruará	Granodiorite	1986 ± 5			(3)

Key to references: (1) Macambira et al. (2004); (2) Santos (2003); (3) Vasquez et al. (2005); (4) Faraco et al. (2005); (5) Macambira et al. (2003); (6) Macambira et al. (2001) and (7) Souza et al. (2003).

[a] Subdivision of the Precambrian recommended by International Union of Geological Sciences, Plumb (1991).

[b] Inherited zircon crystals; (WR) whole rock.

standing of the geological evolution of the Maroni-Itacaiúnas province. In this work, new U–Pb SHRIMP and Pb-evaporation data are presented for rocks from the west part, allowing a new history of the magmatic events of that domain to be compiled, and a comparison to be made with the geological evolution of other Trans-Amazonian terranes of the Amazonian craton.

2. Geological setting

The first models of evolution of the Amazonian Craton were based on K–Ar and Rb–Sr dating obtained during the geological mapping programs carried out in the 1960s and 1970s, which were further updated by few U–Pb, Pb–Pb and Sm–Nd data obtained during the 1980s (e.g. Cordani et al., 1979; Teixeira et al., 1989). In these evolution models, Archean nucleii are surrounded by Paleoproterozoic and Mesoproterozoic geochronological provinces that became progressively younger towards the southwestern edge of the craton. The Central Amazonian province (>2.5 Ga), at the central-southeastern part of the Amazonian Craton, is bounded in the northeast by the Maroni-Itacaiúnas province (2.2–1.95 Ga) and the Ventuari-Tapajós province (1.95–1.8 Ga) to the west. The Maroni-Itacaiúnas province spreads from the northern/northeastern (Guiana shield) to the eastern parts of craton (Fig. 1).

Recent evolutionary models proposed for the Central Amazonian province of the Amazonian craton have distinguished an Archean domain (Carajás block) from that reworked by Paleoproterozoic events (Xingu-Iricoumé block) (Dall'Agnol et al., 1999a; Tassinari and Macambira, 1999, 2004; Tassinari et al., 2000). This Archean domain is composed of Mesoarchean (3.0–2.87 Ga) and Neoarchean (2.76–2.54 Ga) granitoid-greenstone terranes, whereas the basement of the Xingu-Iricoumé block is poorly known due to limited exposure and widespread Orosirian to Statherian (2.0–1.76 Ga) intrusions, and volcanic and sedimentary cover. Other authors have proposed different limits and names for the geochronological provinces of the Amazonian craton. For example, according to Santos (2003) and Santos et al. (2006), the Meso (Rio Maria) and Neoarchean (Carajás) domains, grouped in the Carajás province, extend westwards to the Uruará area. However, Vasquez et al. (2005) dated a Rhyacian granitoid (Table 1 and Fig. 2) in the westernmost part of the region, showing that this segment is part of the Maroni-Itacaiúnas province.

According to recent geological maps and dating (e.g. Delor et al., 2003a; Rosa-Costa et al., 2003), the Maroni-Itacaiúnas province, in the Guiana shield, is made up of Rhyacian ocean-floor tholeiitic magmatism, greenstone belts, TTG, and granitic plutonism, related to the main Trans-Amazonian event (2.26–2.08 Ga), and with associated Archean inliers. In addition, late Rhyacian (2.07–2.05 Ga) granulite belts and batholiths of charnockitic rocks are related to late Trans-Amazonian high-grade tectonometamorphic and magmatic events (Roever et al., 2003; Delor et al., 2003b).

The Bacajá domain is divided into two distinct regions: the eastern part and the west part. For more detailed discussion, each region is divided in several areas. To the south and the west, it borders on the Central Amazonian province, where the Archean Carajás block is included. To the north it is covered by the Phanerozoic Amazon sedimentary basin (Fig. 1), and to the east, the Bacajá domain is bordered by the Neoproterozoic supracrustal rocks of the Araguaia belt.

The Bacajá domain comprises Paleoproterozoic granitoids, supracrustal rocks, high-grade metasedimentry rocks, metaigneous granulites and charnockitic rocks with associated Archean inliers of orthogneisses. Based on Rb–Sr data, Santos et al. (1988) suggested Paleoproterozoic reworking of the gneissic basement and juvenile crust formation of mafic metavolcanic rocks from the west part during the Trans-Amazonian cycle. The reworking of the basement rocks from eastern part of the domain was previous suggested by Silva et al. (1974) and formally proposed by Cordani et al. (1984).

The first U–Pb SHRIMP and Pb-evaporation data indicated the dominance of Rhyacian granitoids and charnockitic rocks with ages between 2.07 and 2.21 Ga as well as local occurrences of Neoarchean and Siderian orthogneiss, supracrustal rocks and granitoids of 2.44–2.67 and 2.31–2.36 Ga, as well as Orosirian granitoids of 1.99 Ga (Macambira et al., 2001, 2003, 2004; Santos, 2003; Faraco et al., 2005; Vasquez et al., 2005). In addition, the Nd isotope data distinguished a juvenile crust of ca. 2.67 Ga and two sources of Rhyacian granitoids (ca. 2.1 Ga) from the eastern part of the Bacajá Domain: a late Siderian juvenile source with T_{DM}Nd ca. 2.3 Ga ($\varepsilon Nd_{(t)} = +0.83$ to -0.6), and a Neoarchean crustal source with T_{DM}Nd ca. 2.6 Ga ($\varepsilon Nd_{(t)} = -4.25$) (Macambira et al., 2004).

3. Geology of the Bacajá domains

Most geological maps of the Bacajá domain grouped the lithologies in formal lithostratigraphic and lithodemic units (Silva et al., 1974, Issler et al., 1974; Jorge João et al., 1987; Oliveira et al., 1994; Faraco et al., 2005). In this work, the rocks are grouped in lithologic associations in order to avoid ambiguous correlations with formal units.

In the west part of the Bacajá domain, the basement is composed of orthogneisses, paragneisses (high-grade metasedimentary rocks), orthogranulites and migmatites. These rocks occur as massifs and enclaves within granitoids. The main occurrences of orthogneisses are in the Uruará, Maribel and Manelão areas, whereas the most extensive body of high-grade metasedimentary rocks and orthogranulites is located in the Ilha Grande and Ipiaçava areas (Fig. 2).

3.1. Orthogneisses

The orthogneisses are light and dark grey-banded gneisses (Fig. 3A) with orthoamphibolite boudins and local migmatitic structures. They are biotite and hornblende bearing metatonalites and metagranodiorites with subordinate metamonzogranites and metaquartz diorites showing polygonal and porphyroclastic textures. These metaluminous orthogneisses do not show metamorphic diagnostic paragenesis, nevertheless the polygonal plagioclase and hornblende, as well the migmatitic features and amphibolite boundins, indicate that they underwent middle amphibolite facies metamorphism (Vasquez et al., 2005).

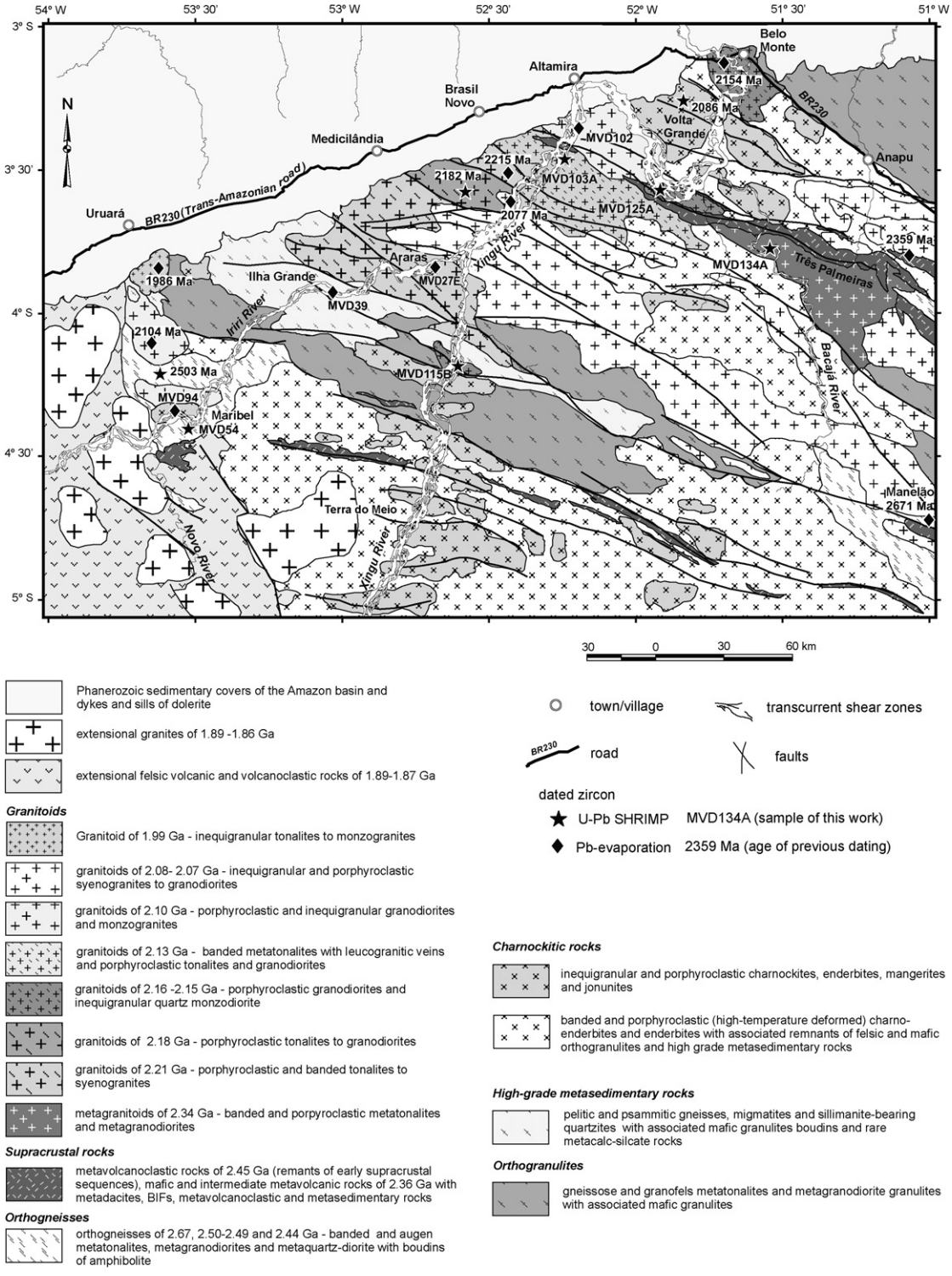

Fig. 2. Geological map of the western Bacajá domain with location of dated samples.

U–Pb SHRIMP and Pb-evaporation zircon ages of 2671 ± 3 and 2440 ± 1 Ma were obtained for these orthogneisses (Table 1).

3.2. Metasedimentary high-grade rocks

The high-grade metasedimentary rocks comprise metapelites, quartz-rich metapsammites and rare metacalc-silicate rocks (described in Santos et al., 1988) with frequent migmatitic structures and boudins (paleo-dykes) of associated mafic granulites. The metasedimentary rocks crop out as usually dark grey gneissose pelites, light grey granofels psammites, mesosomatic augen gneisses with leucosomatic veins of muscovite- and garnet-bearing leucogranites (Fig. 3B). Their mineral assemblages are composed of plagioclase, K-feldspar, quartz, red biotite (Ti-rich), garnet, cordierite and sillimanite that indicate for these a low pressure and high-temperature

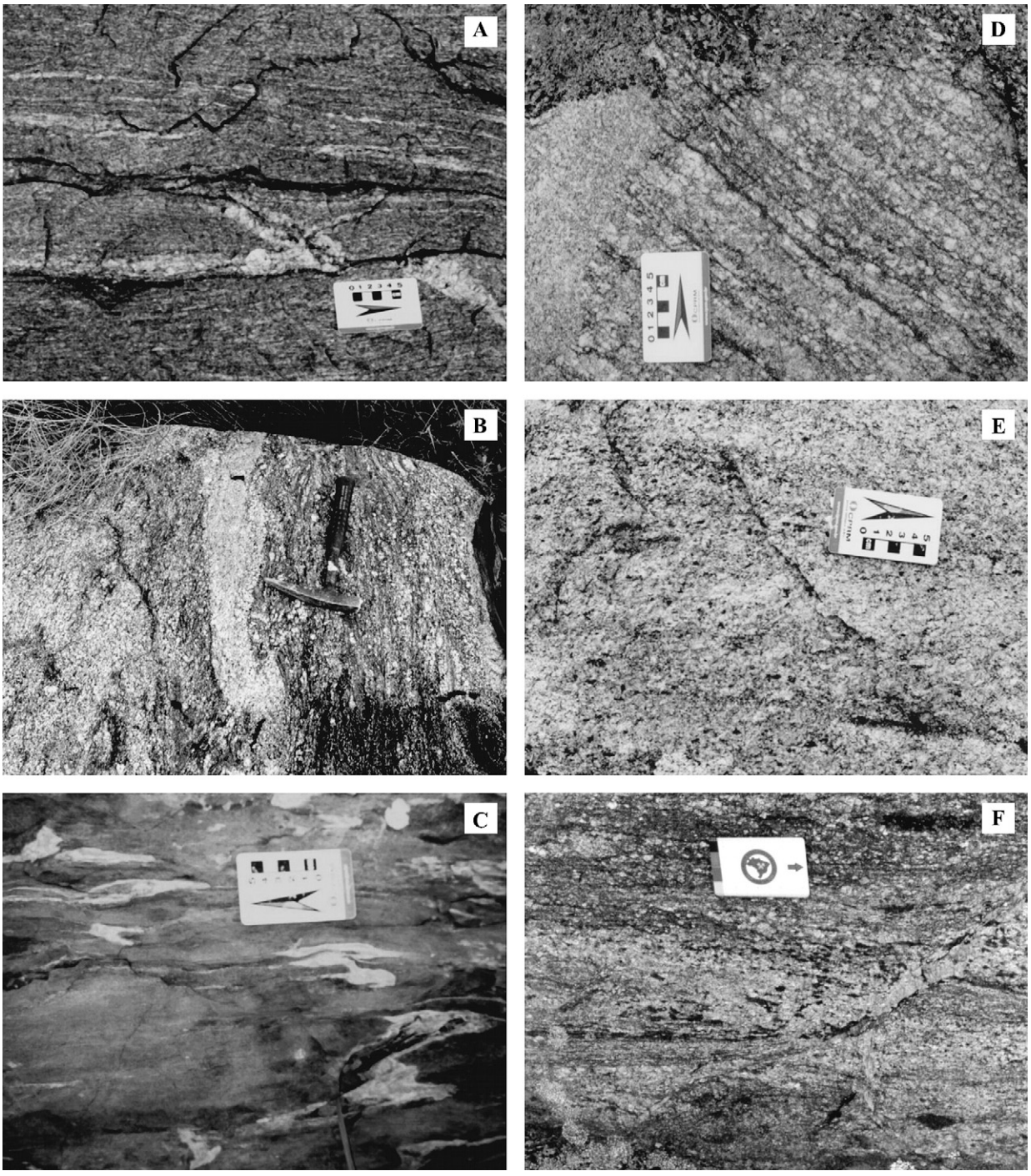

Fig. 3. Mesoscopy features of rocks of the main lithologic associations from the western Bacajá domain. (A) Banded orthogneiss with tightly folded leucogranite veins; (B) leucosomatic vein of garnet- and cordierite-bearing leucogranites in a metapelite; (C) plagioclase-actinolite schist with tightly folded quartz veins (rootless folds); (D) porphyroclastic tonalite cut by granular syenogranite; (E) inequigranular charnockite; and (F) banded orthogranulite.

metamorphism under upper amphibolite to granulite facies metamorphism (Santos et al., 1988; Vasquez et al., 2005). These rocks furnished Pb-evaporation zircon ages between 2361 and 2076 Ma (Table 1).

3.3. Orthogranulites

The granulites of igneous derivation are gneissose and granofels metatonalites and metagranodiorites (Fig. 3F) closely associated with charnockitic igneous bodies and paragneisses. These orthogranulites host centimeter- to meter scale mafic granulite boudins of polygonal granoblastic metagabbro, which probably represent paleo-dykes. Mineral assemblages include plagioclase, K-feldspar, quartz, brownish green hornblende, reddish brown biotite, orthopyroxene and clinopyroxene. Retrograde metamorphic textures of pyroxene as replacement, inclusion and intergrowths are common but locally pyroxenes, hornblende and biotite are in equilibrium (Ricci, 2006b).

Pyroxene-free orthogranulites are common, especially in those bodies strongly affected by mylonitic deformation of transcurrent shear zones. Relicts of pyroxene, antiperthites, mesoperthites and remnant of mafic granulite boudins provide evidence of granulite grade metamorphism in these rocks.

3.4. Supracrustal rocks

The supracrustal sequences are generally elongated bodies parallel to WNW–ESE trend. The Três Palmeiras greenstone belt, in Volta Grande area, is the largest body (Fig. 2). These metavolcano-sedimentary sequences are comprised of metandesites, metabasalts, metadacites, metatuffs, mafic schists (Fig. 3C), amphibolites, BIFs, quartzites, mica-, graphite- and quartz-bearing schists. The metamafic rocks of the Três Palmeiras greenstone belt are transitional between island arc tholeiites and MORBs, showing a paragenesis of greenschist- to amphibolite facies (Jorge João et al., 1987). A Pb-evaporation zircon age of 2359 ± 3 Ma was obtained for metandesite of this greenstone belt (Table 1).

3.5. Granitoids

The granitoids and charnockitic rocks cut the gneissic and granulitic bodies and greenstone belts (Fig. 2). The granitoid batholiths are elongated parallel to the NW–SE transcurrent shear zones (Fig. 2). They are biotite-bearing granodiorites, tonalites and monzogranites with porphyroclastic to granular textures (Fig. 3D) showing magmatic flow overprinted by a mylonitic foliation. A range of zircon ages between 2215 ± 2 and 2069 ± 6 Ma was determined for these granitoids (Table 1). The oldest granitoids (> 2104 Ma) show evidence of deformation at high-temperature (>550 °C), probably resulting from submagmatic flow, whereas the youngest ones show preserved igneous textures and features of solid state deformation at low-temperatures (≤550 °C) related to the NW–SE shear zone (Vasquez et al., 2005).

A granitoid pluton of porphyritic biotite-bearing granodiorites and tonalites showing abundant magma mingling and local deformation at low-temperature yielded a Pb-evaporation zircon age of 1986 ± 5 Ma and was provisionally included in this unit (Table 1).

3.6. Charnockitic rocks

The bodies of charnockitic rock are generally elongated in an E–W trend and are abundant in the Terra do Meio and Volta Grande areas (Fig. 2). Charnockites and enderbites dominate, but charnoenderbites, mangerites and jotunites also occur. There are charnockitic rocks with preserved igneous textures (Fig. 3E) and others showing ductile deformation at low- and high-temperatures. Plagioclase shows blebby to stringy antiperthitic exsolution and mesoperthitic exsolution is frequent in the K-feldspar. Pyroxene break-down reactions are present as rimmed biotite and/or hornblende and fringery biotite intergrown with quartz lenses. Sometimes the mineral is completely replaced (pyroxene-free) or just in form of pseudomorphs after pyroxene (Ricci, 2006a). A charnockite pluton in the Volta Grande area, previously considered as granite, the Belo Monte monzogranite (Santos, 2003), gave a U–Pb SHRIMP age of 2086 ± 5 Ma (Table 1)

Most lithologic associations of the western Bacajá domain also outcrop in the east part. However, orthogranulites and charnockitic rocks are more abundant and their bodies are larger in the eastern Bacajá domain. On the other hand, Rhyacian granitoids and supracrustal rocks are less frequent in this part. In addition, Faraco et al. (2005) have found granitoids with U–Pb SHRIMP zircon ages of 2313 ± 9 and 2114 + 35/−33 Ma (Table 1) in the east part of the Bacajá domain, which have not yet been found in the west part.

4. Geochronology

4.1. Analytical procedures

Zircon crystals were dated by single zircon Pb-evaporation and U–Pb SHRIMP methods. The mineral separation and Pb-evaporation analyses were carried out at the Isotope Geology Laboratory (Pará-Iso) of the Federal University of Pará, Belém, Brazil. Zircon concentrates were extracted using gravimetric (dry shaking table and heavy liquids) and magnetic (isodynamic separator) techniques. The analyzed grains were selected by handpicking under a stereomicroscope.

Pb-evaporation analyses were undertaken using the ion-counting system of a Finnigan MAT 262 mass spectrometer in dynamic mode. The procedures of the Pb-evaporation method are described in Kober (1986, 1987) and the data treatment was based on Gaudette et al. (1998). Zircon grains were dated at increasing evaporation temperatures and an age was calculated from the average of the $^{207}Pb/^{206}Pb$ ratios for each evaporation step. Initial common lead corrections were base on the Stacey and Kramers (1975) model and blocks with $^{206}Pb/^{204}Pb$ ratios lower than 2500 were usually eliminated from any age calculation in order to minimize the common lead interference. The crystallization age of each sample was calculated using the mean value of the $^{207}Pb/^{206}Pb$ ratios at the highest temperature steps (preferably > 1450 °C) and at least three grains were used to define the age of each sample. Crystals with lower ages which could reflect Pb-loss after crystallization, as well as grains showing higher ages and considered as inherited, were rejected and not included in the calculation of a mean age. The effect of mass fractionation on the $^{207}Pb/^{206}Pb$ ratios was corrected using a factor of 0.12% ± 0.03 per amu, determined by repeated analyses of the NBS-983 standard. Pb-evaporation ages presented in this study are quoted with 2σ uncertainties.

U–Pb SHRIMP analyses were undertaken on SHRIMP II and RG of the Research School of Earth Sciences of the Australian National University, Canberra, Australia. Zircon crystals were hand-picked, mounted in epoxy resin, ground to half-thickness, and polished with 3 and 1 μm diamond paste; a conductive gold-coating was applied just prior to analysis. The grains were photographed in reflected and transmitted lights, and cathodoluminescence (CL) images were produced in a scanning electron microscope in order to investigate the internal structures of

the zircon crystals and to characterize different populations. SHRIMP analytical procedures followed the methods described in Compston et al. (1984) and Williams (1998). The standard zircon SL13 (Claoué-Long et al., 1995) was used to determinate U concentration and the U–Pb ratios were referenced to the zircon standard FC1 (Paces and Miller, 1993). Raw isotopic data were reduced using the Squid program (Ludwig, 2001), and age calculations and concordia plots were done using both Squid and Isoplot/Ex software (Ludwig, 2003). Analyses and ages for individual SHRIMP spots are listed in the data tables and plotted on concordia diagrams with 1σ uncertainties. Where data are combined to calculate an age, the quoted uncertainties are at 95% confidence level, with uncertainties in the U–Pb standard calibration included in any relevant U–Pb intercept and concordia age calculations.

4.2. Sample descriptions and results

Sampling in the western Bacajá domain (Fig. 2) was focus on orthogneisses of amphibolite facies, granitoids and charnockitic rocks in order to investigate magmatic events.

4.2.1. Granodioritic gneiss MVD54

Sample MVD54 is a light gray, banded orthogneiss from the Maribel area (Fig. 2) with tightly folded leucogranitic veins (Fig. 3A). It is a biotite-bearing metagranodiorite showing inequigranular and polygonal arrays overprinted during low-temperature deformation by a mylonitic fabric. Epidote, allanite, white mica and chlorite make up the retrograde metamorphic mineral assemblage. Zircon crystals are light yellow, with a range of euhedral to anhedral forms, with both long and short prisms, and with pyramidal terminations showing oscillatory zoning. Rounded cores are present (Fig. 4A). Many grains show dark rims (in CL) of various sizes which clearly overgrow or truncate earlier magmatic growth zones (Fig. 4A and B).

Most SHRIMP analyses produced highly discordant and scattered data (Table 2; Fig. 5A). The majority of the discordant data follow a rough discordia trend suggesting recent Pb-loss. Data which scatter about this trend or which clearly fall off this trend have a more complex history which could be due to multistage Pb-loss, or to some original heterogeneity in the age of the zircons.

The local occurrence of migmatitic features in this orthogneiss could suggest a reworking, probably during the Trans-Amazonian cycle, but again this is not clear from the geochronological results. Three analyses (8.2, 13.1 and 18.1) sited within the dark CL overgrowths described earlier (and shown in Fig. 4B) have very high U contents and low Th–U ratios (~0.03) characteristic of metamorphic zircon. Unfortunately, the analyses are also highly discordant and no definite age can be obtained for this late-stage generation of growth. Thus, a Trans-Amazonian age for metamorphism/migmatization could be possible, but clearly better zircon would be required to define unequivocally the age of such an event.

In order to establish an age for this orthogneiss, only the least discordant data (<10%) were considered. These data (shown in Fig. 5A) are all from the oscillatory-zoned phase interpreted to represent the magmatic zircon (Fig. 4B). Although there is still some scatter of these data (a result of early Pb-loss?), an upper intercept age of 2487 ± 13 Ma can be calculated. This is interpreted as the best approximation of the age of crystallization for the protolith of this granodioritic gneiss. Two near-concordant data with $^{207}Pb/^{206}Pb$ ages of 2548 ± 6 (2.1) and 2521 ± 14 Ma (10.1) were sited in rounded cores and are interpreted as representing an inherited or xenocrystic components (Fig. 4A).

4.2.2. Dacitic metalapilli-tuff MVD39

A decameter-sized xenolith of metavolcanoclastic felsic rock (sample MVD39) is hosted in high-grade metasedimentary rocks from the Ilha Grande area (Fig. 2). It is a dacitic metalapilli with intercalated centimeter- to millimeter-thick layers of metatuffites. White mica-rich layers mark the foliation. The main zircon population is light pink, with short pyramids and rounded rims and cores. All analyzed grains gave Pb-evaporation step ages between 2410 and 2455 Ma at heating steps of 1500 and 1550 °C (Table 3) and four crystals yielded a mean age of 2452 ± 3 Ma (Fig. 6A), which is interpreted as the minimum age of crystallization for the igneous protolith (dacite autoclasts) of the dacitic metalappilli-tuff.

4.2.3. Metatonalite MVD134A

A banded porphyroclastic metatonalite (sample MVD134A) with boudins of metamafic dykes border the Três Palmeiras greenstone belt (Fig. 2). The submagmatic fabric is partially overprinted by a low-temperature mylonitic fabric. The zircon crystals from this sample consist of short pyramids and long prisms, are light yellow and colorless, have few inclusions, and show euhedral oscillatory zoning typical of magmatic zircon (Fig. 4C). The eight near-concordant data yield a concordia age of 2338 ± 5 Ma (Fig. 5C; Table 4), interpreted as the crystallization age of the tonalite.

4.2.4. Porphyroclastic syenogranite MVD27E

Sample MVD27E is a foliated porphyroclastic biotite syenogranite from the Araras area (Fig. 2) with preserved igneous texture, despite the strong high-temperature deformation typically found in these granitoids. Zircon crystals are euhedral and subhedral, elongated prisms and equant pyramids, light pink and pale yellow, and many of which contain numerous cracks and inclusions. The mean age calculated from three best grains (crystals 1, 2 and 3) as concern Pb-loss at heating step of 1500 °C is 2210 ± 3 Ma. Another analysis (crystal 4) gave a similar result, but with a $^{206}Pb/^{204}Pb$ ratio slight lower than that considered acceptable (Table 3). Inclusion of this analysis in the calculated mean gives a crystallization age of 2209 ± 2 Ma (Fig. 6B).

4.2.5. Porphyritic quartz-monzodiorite MVD125A

Sample MVD125A is another Rhyacian granitoid with well-preserved igneous textures, but is locally affected by shear zones. It was collected from a pluton of porphyritic quartz-monzodiorite with strong hydrothermal alteration related to

Table 2
Summary of SHRIMP U–Pb zircon data for sample MVD54

Grains spot	^{206}Pb (%)	U (ppm)	Th (ppm)	^{232}Th/^{238}U	^{206}Pb* (ppm)	^{206}Pb/^{238}U age[a] (Ma)	^{207}Pb/^{206}Pb age[a] (Ma)	Percentage discordant	^{207}Pb*/^{206}Pb*[a]	± (%)	^{207}Pb*/^{235}U[a]	± (%)	^{206}Pb*/^{238}U[a]	± (%)	Errors correlation
1.1	2.04	210	100	0.49	45.9	1435 ± 10	2422 ± 32	41	0.1569	1.9	5.391	2.01	0.2493	0.78	0.386
2.1	0.03	210	134	0.66	88.5	2571 ± 16	2548 ± 6	−1	0.1691	0.37	11.423	0.83	0.4900	0.75	0.894
3.2	0.02	164	121	0.76	67.4	2159 ± 15	2490 ± 6	−1	0.1633	0.38	10.767	0.81	0.4782	0.72	0.882
3.3	0.09	1647	297	0.19	431	1711 ± 10	2421 ± 29	29	0.1567	1.7 4	6.570	1.86	0.3041	0.67	0.360
4.1	0.11	445	279	0.65	167	2333 ± 18	2488 ± 5	6	0.1631	0.30	9.807	0.97	0.4361	0.92	0.952
5.1	1.12	467	72	0.16	113	1589 ± 9	2454 ± 17	35	0.1598	0.99	6.159	1.19	0.2795	0.66	0.556
5.2	1.23	1099	731	0.69	233	1404 ± 15	2339 ± 18	40	0.1494	1.07	5.015	1.57	0.2434	1.15	0.734
6.1	0.09	51	46	0.94	19.2	2347 ± 21	2480 ± 14	5	0.1623	0.82	9.831	1.35	0.4392	1.08	0.797
6.2	0.20	35	21	0.63	13.7	2419 ± 25	2501 ± 19	3	0.1644	1.11	10.322	1.66	0.4554	1.22	0.740
7.1	0.00	152	58	0.39	61.8	2501 ± 16	2486 ± 7	−1	0.1629	0.42	10.646	0.88	0.4739	0.77	0.879
7.2	0.07	134	60	0.46	54.4	2492 ± 16	2509 ± 13	1	0.1652	0.78	10.747	1.08	0.4719	0.76	0.698
8.1	1.15	104	36	0.36	19.4	1256 ± 10	2464 ± 25	49	0.1608	1.47	4.768	1.72	0.2151	0.89	0.515
8.2	1.81	2036	60	0.03	308	1027 ± 6	1736 ± 38	41	0.1062	2.07	2.529	2.16	0.1726	0.61	0.281
9.1	0.34	293	102	0.36	109	2310 ± 13	2456 ± 8	6	0.1600	0.47	9.508	0.83	0.4310	0.69	0.826
10.1	0.00	62	38	0.63	26.2	2582 ± 22	2521 ± 14	−2	0.1663	0.85	11.295	1.34	0.4925	1.04	0.773
10.2	4.28	108	38	0.36	27.5	1613 ± 22	2467 ± 28	35	0.1611	1.65	6.315	1.88	0.2843	0.90	0.479
11.1	0.01	161	31	0.20	66.4	2531 ± 17	2466 ± 8	−3	0.1610	0.45	10.676	0.92	0.4810	0.80	0.873
12.1	1.16	1107	256	0.24	317	1836 ± 10	2442 ± 16	25	0.1587	0.97	7.214	1.16	0.3296	0.64	0.550
13.1	0.55	2394	76	0.03	373	1069 ± 11	1883 ± 16	43	0.1152	0.88	2.866	1.43	0.1804	1.09	0.779
14.1	0.48	224	59	0.27	72.8	2064 ± 13	2540 ± 10	19	0.1682	0.60	8.753	0.95	0.3774	0.74	0.773
14.2	2.73	460	145	0.33	114	1594 ± 14	2370 ± 42	33	0.1521	2.47	5.882	2.66	0.2804	1.01	0.377
15.1	0.46	188	98	0.54	48.9	1699 ± 31	2461 ± 15	31	0.1605	0.88	6.672	2.24	0.3015	2.06	0.920
16.1	0.19	380	76	0.21	127	2114 ± 12	2394 ± 7	12	0.1543	0.41	0.256	0.78	0.3881	0.66	0.853
17.1	1.03	92	21	0.23	15.3	1125 ± 11	2405 ± 28	53	0.1553	1.66	4.083	1.97	0.1906	1.06	0.537
18.1	0.23	1949	76	0.04	395	1363 ± 12	1820 ± 8	25	0.1112	0.43	3.612	1.09	0.2355	1.00	0.918
19.1	4.03	1699	257	0.16	190	758 ± 5	2007 ± 73	62	0.1235	4.14	2.125	4.21	0.1248	0.77	0.183
20.1	0.53	450	188	0.43	163	2255 ± 13	2410 ± 10	6	0.1558	0.58	8.993	0.88	0.4187	0.66	0.754
21.1	0.72	304	51	0.17	84.6	1800 ± 16	2462 ± 14	27	0.1606	0.84	7.131	1.31	0.3221	1.01	0.769
22.1	1.18	537	162	0.31	141	1698 ± 9	2403 ± 7	29	0.1551	0.43	6.446	0.73	0.3015	0.58	0.804
23.1	0.87	760	24	0.03	177	1531 ± 8	2171 ± 15	29	0.1356	0.89	5.010	1.09	0.2681	0.57	0.538
24.1	0.31	235	77	0.34	79	2122 ± 12	2468 ± 7	14	0.1611	0.42	8.661	0.78	0.3898	0.66	0.846
25.1	6.50	891	219	0.25	91.5	683 ± 5	2222 ± 22	69	0.1396	1.28	2.149	1.49	0.1117	0.75	0.505
26.1	0.03	243	128	0.54	91.2	2334 ± 13	2462 ± 9	5	0.1606	0.52	9.664	0.84	0.4364	0.66	0.786
27.1	0.18	235	82	0.36	84.3	2242 ± 13	2462 ± 6	9	0.1606	0.37	9.210	0.76	0.4159	0.66	0.873
28.1	0.10	357	145	0.42	137	2384 ± 12	2470 ± 7	3	0.1613	0.44	9.956	0.75	0.4476	0.61	0.808
29.1	0.04	152	104	0.71	61.5	2481 ± 15	2501 ± 8	1	0.1644	0.45	10.643	0.87	0.4695	0.74	0.853
30.1	0.00	141	114	0.83	56.9	2483 ± 15	2466 ± 7	−1	0.1609	0.41	10.427	0.86	0.4699	0.75	0.876

Errors are 1σ; Pb* indicate the radiogenic portion. Error in standard calibration was 0.19% (not included in above errors but required when comparing data from different mounts).

[a] Common Pb corrected using measured ^{204}Pb.

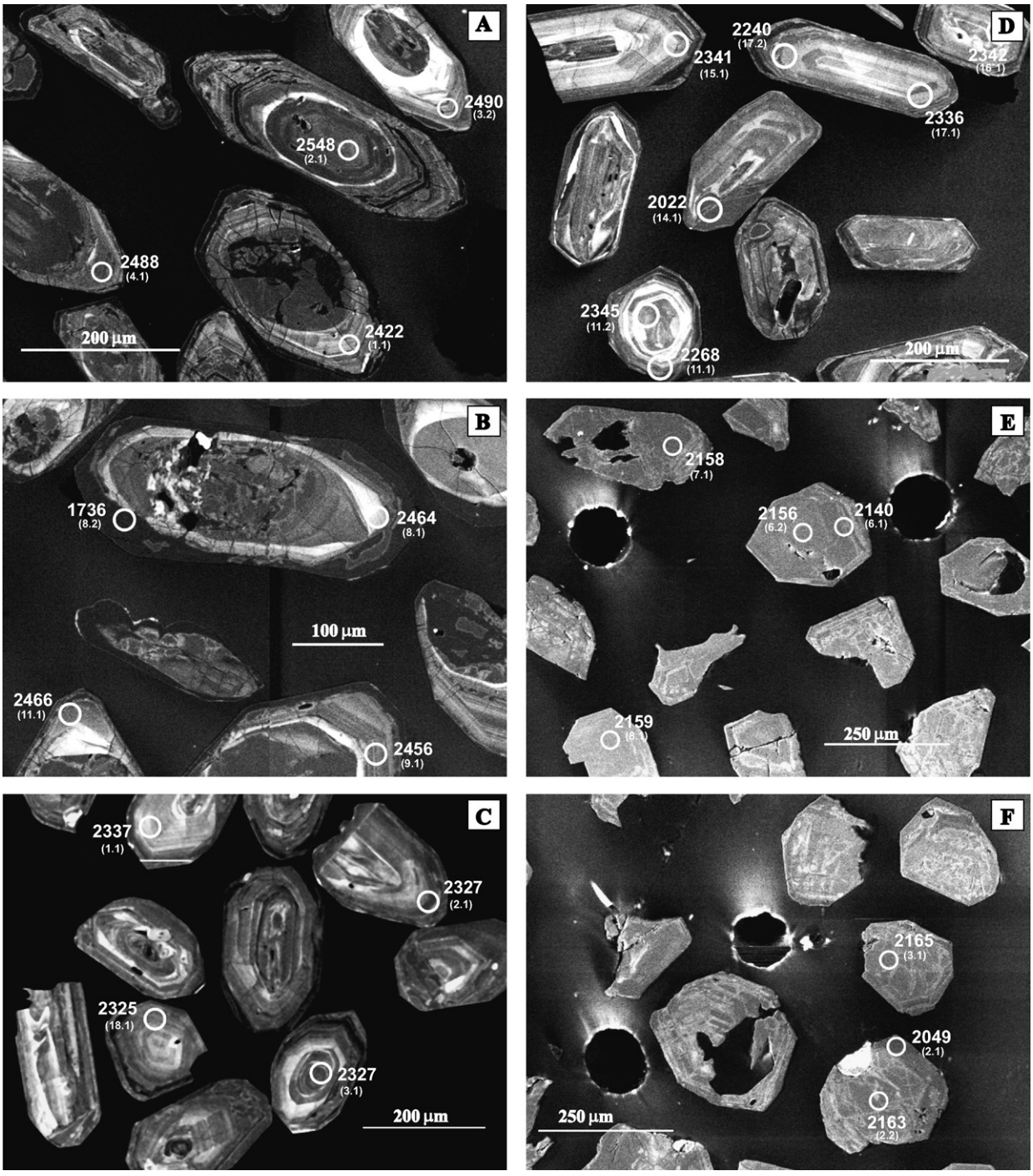

Fig. 4. Cathodoluminescence images of analyzed zircon crystals of the samples MVD54 (A and B), MVD134A (C and D) and MVD125A (E and F), with the ion microprobe spots, their number in the parentheses and respective $^{207}Pb/^{206}Pb$ ages.

gold mineralization that cuts the Três Palmeiras greenstone belt (Fig. 2). Zircon morphology is uniform with euhedral equant pyramids, brownish and grayish grains with few inclusions. In CL images these zircon crystals show weak oscillatory zoning (Fig. 4E) and many have U-rich patches and rims (Fig. 4F). Discordant data are from U- and Th-rich crystals (Table 5) but this enrichment did not affect the age result. The near-concordant analyses gave a mean $^{207}Pb/^{206}Pb$ age of 2160 ± 3 Ma (Fig. 5D), interpreted as the crystallization age of the quartz-monzodiorite pluton.

4.2.6. Porphyroclastic monzogranite MVD115B

Porphyroclastic granitoids intrude the high-grade metamorphic and associated charnockitic rocks. In the central part of the study area (Fig. 2) there is a porphyroclastic biotite monzogranite (sample MVD115B) with disrupted and boudined leucogranite veins showing microtextures of high-temperature deformation. Zircon crystals are light yellow and colorless, euhedral long prisms and short pyramids, have many inclusions and few fractures. Most grains show euhedral oscillatory zoning, but there are crystals with dark CL zones, probably altered

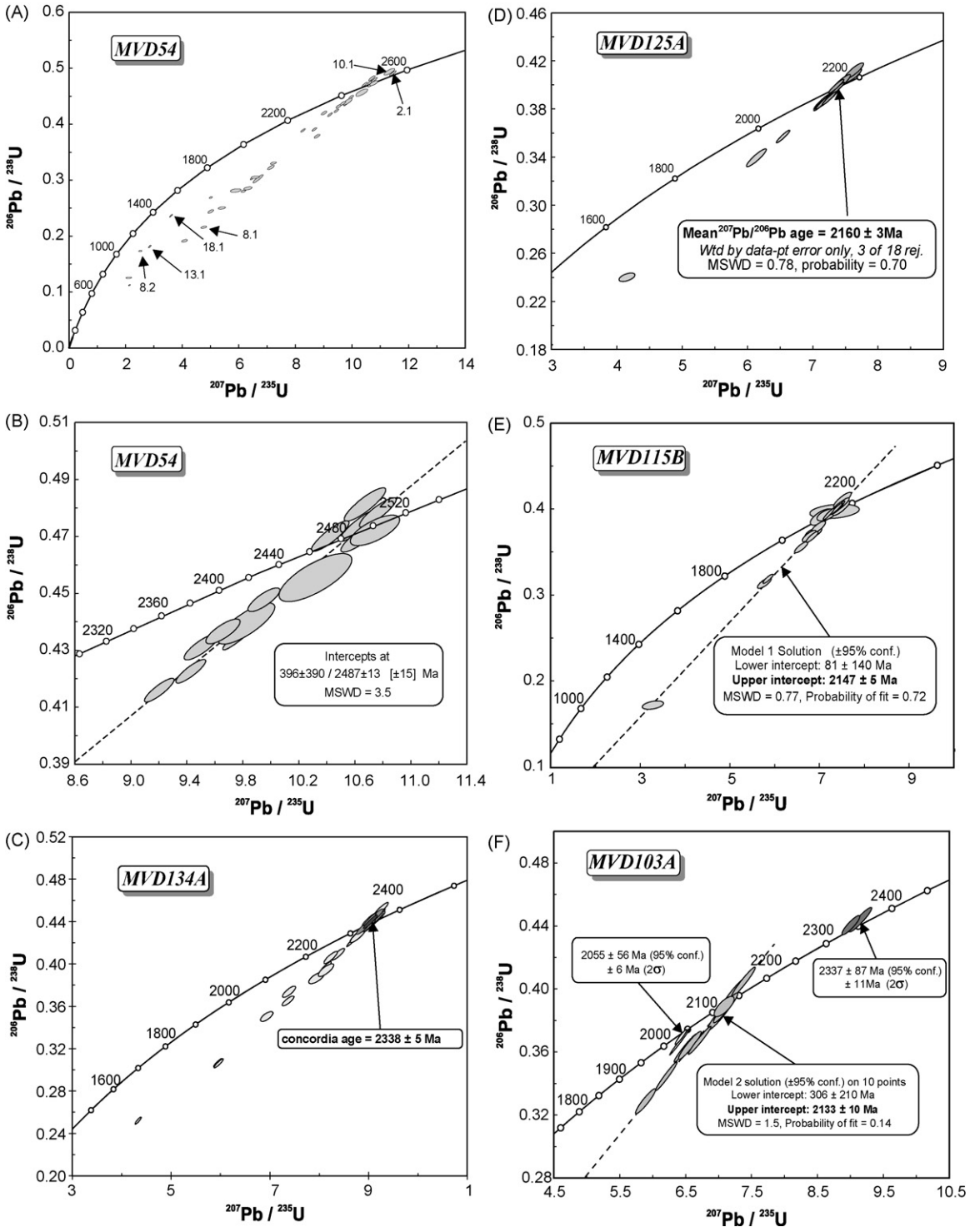

Fig. 5. Concordia plots of the samples MVD54 (A and B), MVD134A (C), MVD125A (D), MVD115B (E) and MVD103A (F).

or metamict patches and rims, where planar oscillatory zoning is erased (Fig. 7A and B). A number of the SHRIMP analyses are highly discordant (Table 6) but regression of all data yielded a Model 1 solution with an upper intercept age of 2147 ± 5 Ma (Fig. 5E), here interpreted as the crystallization age of this monzogranite pluton.

4.2.7. Metatonalite MVD103A

Rhyacian granitoids are abundant in the northern part of the study area (Fig. 2) and the type of deformation is varied. Sample MVD103A is a greenish gray metatonalite with banding and folded leucogranite veins, which under the microscope shows feldspars and quartz in polygonal array and biotite strongly

Table 3
Summary of Pb-evaporation isotopic data on zircon of rocks from the western Bacajá domain

Zircon	T (°C)	No. of ratios	$^{206}Pb/^{204}Pb$	$^{208}Pb/^{206}Pb$	2σ	$^{207}Pb/^{206}Pb$	2σ	$^{207}Pb/^{206}Pb$[a]	2σ	Step age (Ma)	2σ
Sample MVD39, dacitic metalapilli-tuff[b]											
1	1450	36	6,410	0.14565	91	0.15596	98	0.15399	102	2391	11
	1500	**14**	**55,556**	**0.18336**	**123**	**0.15943**	**109**	**0.15923**	**11**	**2448**	**12**
3	**1500**	**22**	**30,303**	**0.15823**	**59**	**0.16018**	**38**	**0.15977**	**42**	**2454**	**4**
4	1450	6	61	0.99559	1164	0.37088	94	0.19461	43	2782	36
5	**1500**	**30**	**45,455**	**0.04483**	**81**	**0.15952**	**57**	**0.15931**	**61**	**2449**	**6**
6	1450	30	58,824	0.13580	228	0.15034	494	0.14965	48	2342	55
8	**1550**	**12**	**30,303**	**0.14964**	**213**	**0.16044**	**105**	**0.15993**	**86**	**2455**	**9**
9	1450	8	4,464	0.19592	1241	0.15852	537	0.15567	539	2410	59
	1500	4	3,484	0.18063	659	0.15994	45	0.15630	46	2416	5
10	1450	8	2,7778	0.02593	198	0.17626	1245	0.17581	1245	2614	118
	1500	14	76,923	0.03088	248	0.15355	197	0.15338	197	2384	22
	1550	6	>100,000	0.03209	256	0.15673	298	0.15673	298	2421	32
11	1450	20	>100,000	0.07873	5688	0.15158	267	0.15158	267	2364	30
12	1450	16	6,098	0.07734	421	0.15421	93	0.15238	932	2373	104
	1500	20	4,808	0.06587	49	0.15835	51	0.15571	53	2410	6
Sample MVD27E, porphyroclastic syenogranite[c]											
1	**1500**	**34**	**4,274**	**0.12706**	**145**	**0.14163**	**36**	**0.13861**	**41**	**2210**	**5**
2	1450	16	323	0.20194	304	0.17172	71	0.13049	137	2105	18
	1500	**38**	**6,579**	**0.1214**	**102**	**0.14054**	**45**	**0.13866**	**38**	**2211**	**5**
3	**1500**	**36**	**1,410**	**0.14285**	**56**	**0.14725**	**36**	**0.13828**	**34**	**2206**	**4**
4	**1500**	**12**	**4,348**	**0.13477**	**61**	**0.14149**	**32**	**0.13855**	**37**	**2209**	**5**
5	1450	22	2,028	0.08634	61	0.13106	27	0.12474	33	2026	5
6	1450	16	113	0.28003	693	0.24918	189	0.13169	405	2124	53
7	1450	8	509	0.08518	233	0.11232	69	0.08476	102	1310	23
Sample MVD102, porphyroclastic granodiorite[d]											
2	1500	6	>100,000	0.12419	1615	0.13211	661	0.13211	661	2127	88
3	**1480**	**8**	**26,316**	**0.13645**	**309**	**0.13047**	**60**	**0.12997**	**63**	**2098**	**8**
4	1450	4	8,850	0.15566	3152	0.12819	235	0.12669	235	2053	33
	1500	6	**>100,000**	**0.23149**	**215**	**0.13064**	**148**	**0.13064**	**148**	**2107**	**20**
5	1500	38	3,021	0.09946	86	0.13231	35	0.12820	26	2074	4
	1550	**32**	**13,158**	**0.12688**	**225**	**0.13217**	**55**	**0.13046**	**46**	**2104**	**6**
6	1470	8	549	0.16519	728	0.14029	157	0.1158	342	1893	53
8	**1500**	8	>100,000	0.25900	2125	0.13307	419	0.13307	419	2139	55
9	**1500**	**14**	**5,988**	**0.12280**	**92**	**0.13176**	**3**	**0.12975**	**68**	**2095**	**9**
10	**1450**	**8**	**20,000**	**0.29912**	**161**	**0.13055**	**72**	**0.12989**	**75**	**2097**	**10**
12	1450	**16**	**9,615**	**0.11657**	**756**	**0.13232**	**63**	**0.13095**	**81**	**2111**	**11**
13	1450	4	2,933	0.14167	238	0.13397	46	0.12946	65	2091	9
	1500	**34**	**12,500**	**0.12295**	**174**	**0.13138**	**22**	**0.13032**	**23**	**2103**	**3**
	1550	8	>100,000	0.11286	69	0.13146	292	0.13146	292	2118	39
14	1450	40	16,949	0.08044	52	0.12991	29	0.12911	22	2086	3
Sample MVD94, inequigranular jotunite[e]											
1	1450	32	5,051	0.19175	504	0.13012	36	0.12724	31	2061	4
	1500	**40**	**32,258**	**0.08407**	**43**	**0.12828**	**22**	**0.12787**	**24**	**2069**	**3**
	1550	8	**>100,000**	**0.08800**	**589**	**0.12752**	**43**	**0.12752**	**43**	**2064**	6
2	1450	38	4,630	0.24572	243	0.12937	66	0.12684	51	2055	7
	1500	**12**	**>100,000**	**0.11127**	**242**	**0.12793**	**68**	**0.12793**	**68**	**2070**	9
3	1450	30	6,061	0.14731	79	0.12939	18	0.12701	36	2057	5
	1500	**8**	12,346	**0.14405**	**118**	**0.12938**	**96**	**0.12831**	**97**	**2075**	**13**
4	1450	40	83,333	0.15520	88	0.12764	22	0.12747	21	2064	3
	1500	**38**	**250,000**	**0.16627**	**43**	**0.12771**	**20**	**0.12766**	**20**	**2066**	**3**
9	1450	34	2,653	0.17120	979	0.12903	32	0.12495	106	2028	15
	1500	40	4,444	0.12283	152	0.12964	26	0.12650	27	2050	4
10	1450	**30**	6,757	0.19993	234	0.12901	27	0.12735	71	2062	10
	1500	30	**15,385**	**0.12218**	**97**	**0.12895**	**24**	**0.12816**	**38**	**2073**	5
11	1450	38	17,544	0.18553	133	0.12857	34	0.12779	41	2068	6
	1500	**38**	**3,7037**	**0.12407**	**72**	**0.12861**	**28**	**0.12829**	**25**	**2075**	**3**
12	**1450**	**36**	**4,7619**	**0.15894**	**216**	**0.12822**	**37**	**0.12803**	**30**	**2071**	**4**

Bold values denote step used in the mean age.

[a] Common lead corrected according to Stacey and Kramers (1975).

[b] Mean age (crystals 1, 3, 5 and 8; 78 ratios) 2452 ± 3 Ma/MSWD = 0.96.

[c] Mean age (crystals 1, 2, 3 and 4; 120 ratios) 2209 ± 2 Ma/MSWD = 0.98 (mean age calculated with $^{206}Pb/^{204}Pb > 1250$).

[d] Mean age (crystals 3, 4, 5, 9, 10, 12 and 13; 118 ratios) 2102 ± 3 Ma/MSWD = 1.08.

[e] Mean age (crystals 1, 2, 3, 4, 10, 11 and 12; 196 ratios) 2070 ± 3 Ma/MSWD = 1.34.

recrystallized. It appears to be an orthogneiss or granitoid with high-temperature deformation that was strongly affected by mylonitic deformation at low-temperature related to transcurrent shear zones. Zircon morphology is varied in this metatonalite; the main population comprises light yellow, euhedral, equant pyramids and prisms with oscillatory zoning (Fig. 7C and D). Other populations are made up of light brown, subhedral and rounded zircon crystals without well-defined rim-and-core structures and colorless, long prisms showing weak oscillatory zoning (Fig. 7C). Nine analyses of the main population (Table 7) furnished an upper intercept age of 2133 ± 10 Ma (Fig. 5F), interpreted as the crystallization age of the tonalite. There are two other age populations of near-concordant points (Fig. 5F): two zircon crystals with a mean $^{207}Pb/^{206}Pb$ age around 2337 Ma and another two zircon crystals with a mean $^{207}Pb/^{206}Pb$ age around 2055 Ma. The first group is interpreted as inherited, and the younger group is probably related to the formation of leucogranite veins or resetting (Pb-loss) associated with the high-temperature event.

4.2.8. Porphyroclastic granodiorite MVD102

Sample MVD102 is a porphyroclastic granitoid with preserved igneous texture collected in the northern part of study area (Fig. 2). It is a biotite-hornblende granodiorite showing a strong magmatic foliation overprinted by a sub paralleled low-temperature mylonitic foliation. Zircon crystals are dominantly light pink, transparent, euhedral and with a few rounded long prisms with oscillatory zoning, inclusions and fractures. Most grains gave $^{207}Pb/^{206}Pb$ ages around 2100 Ma at heating steps of 1480 and 1550 °C (Table 3). A mean age of 2102 ± 3 Ma was calculated for this granodiorite body from the analysis of seven crystals (Fig. 6C).

4.2.9. Inequigranular jotunite MVD94

In the Maribel area (Fig. 2) there is a charnockitic pluton intruded into orthogneiss with preserved igneous features. It is an inequigranular jotunite (sample MVD94), slightly recrystallized at low-temperature and showing some microtextural evidence of replacement of pyroxenes. Two zircon populations were distinguished: grayish, subhedral and anhedral grains, long prisms, usually striated and cracked, and light pink and pale yellow, short pyramids, with rounded cores, euhedral rims and slightly rounded terminations. Seven crystals from both populations, just one at 1450 °C, furnished a mean age of 2070 ± 3 Ma (Table 3; Fig. 6D).

5. Discussion and interpretations

5.1. Magmatic events

From the zircon geochronology it now possible to distinguish several magmatic events in the Bacajá domain: a Neoarchean

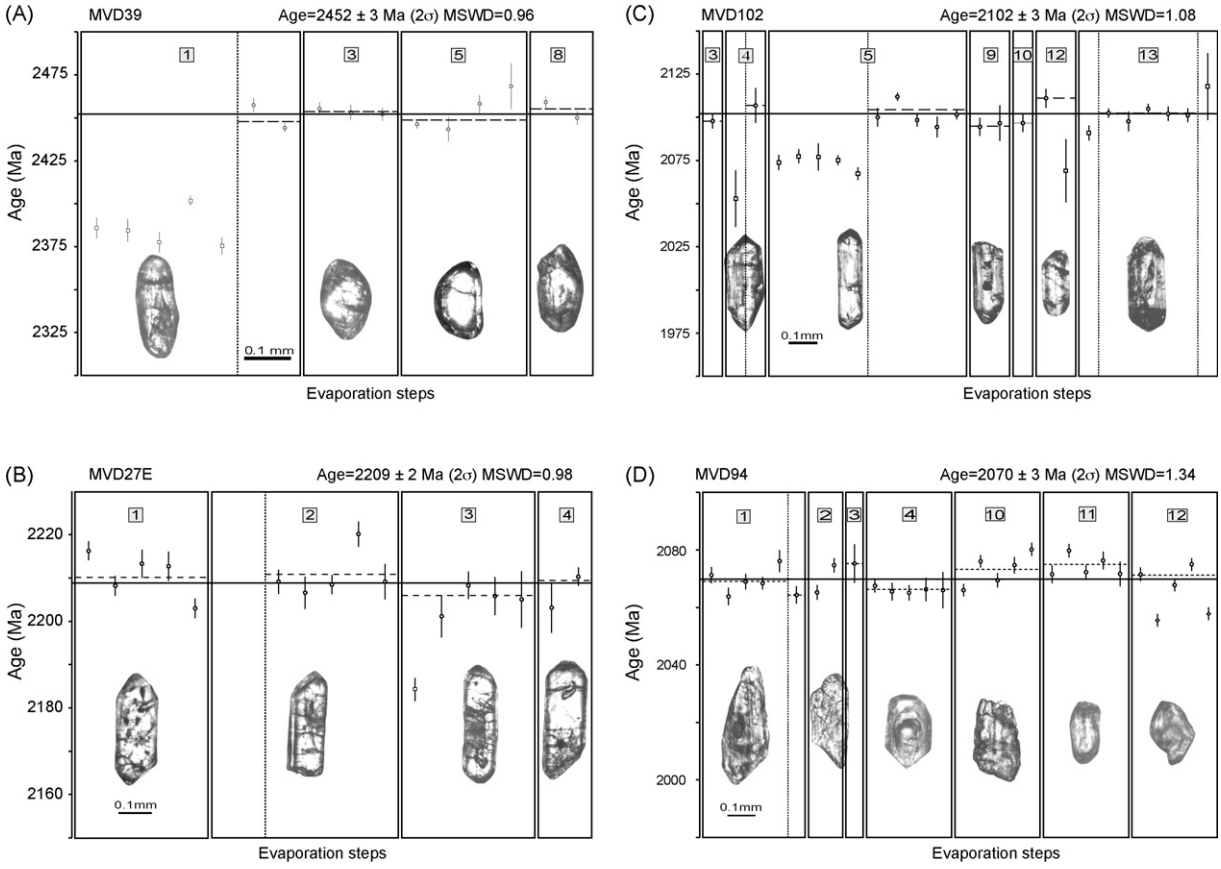

Fig. 6. Diagrams of age vs. evaporation steps of the zircon crystals of the samples MVD39 (A), MVD27E (B), MVD102 (C) and MVD94 (D). Blocks of isotopic ratios used in the calculated of the age (◯), blocks subjectively rejected (□) and because present $^{206}Pb/^{204}Pb$ lower than 2500 (×).

magmatism at 2.67 Ga, early Siderian events of 2.50–2.49 and 2.45–2.44 Ga, late Siderian magmatic events (Table 8). The youngest magmatic event of Orosirian age is 1.99 Ga and only occurs locally with limited distribution.

In the Manelão area (Fig. 2), Macambira et al. (2004) found a tonalitic gneiss of 2671 Ma with Nd isotope data (Table 1), which indicate formation of juvenile Neoarchean crust.

The orthogneisses from the Uruará and Maribel areas (Fig. 2) have magmatic ages between 2503 and 2487 Ma and inherited zircon populations between 2580 and 2520 Ma, which suggest Neoarchean crustal source or xenocrysts assimilated by a juvenile magma.

To east, there is a mega-enclave of metavolcanoclastic rock of 2452 Ma (sample MVD39), probably tectonically imbricated within high-grade metasedimentary rocks from the Ilha Grande area (Fig. 2), and a xenolith of the metaquartz-diorite of 2440 Ma (Vasquez et al., 2005) hosted in a Rhyacian granitoid from the Brasil Novo area. The gap of ca. 50 Ma from the ca. 2.5 Ga event indicates that these remnants represent another early Siderian magmatic event (Table 8).

The juvenile source of 2.67 Ga orthogneiss suggest that this granitoid could be related to island arc whereas crustal traces of the 2.5–2.49 Ga orthogneisses may represent granitoids from magmatic arc bordering a Neoarchean nuclei (microcontinent?). The dacitic and quartz-dioritic composition of 2.45–2.44 Ga rocks suggest that they are also related to magmatic arc.

The Neoarchean to early Siderian magmatic rocks from the Bacajá domain contrast with the most of the Archean orthogneisses and granitoids from the Carajás block, which usually are older (2.74–3.0 Ga, e.g. Tassinari et al., 2000) and have T_{DM} around 3.0 Ga (Sato and Tassinari, 1997; Dall'Agnol et al., 1999b; Rolando and Macambira, 2003; Barros et al., 2004).

Late Siderian magmatic event was detected in the Três Palmeiras area (Fig. 2) is represented by the metandesites of the Três Palmeiras greenstone belt with Pb-evaporation age of 2359 Ma (Macambira et al., 2004) and the associated banded metatonalite (sample MVD134A) of 2338 Ma. This metatonalite of 2.34 Ga has a close spatial and temporal relationship with Três Palmeiras greenstone belt, which has tholeiitic metamafic rocks related to an island arc and ocean floor (Jorge João et al., 1987), suggesting a juvenile character for these late Siderian rocks.

There is also a granitoid of 2313 Ma (Faraco et al., 2005) associated with orthogranulites and Rhyacian charnockitic plutons from the eastern Bacajá domain, but the relationship with 2.36–2.34 Ga magmatism is not clear. However, the 2.31 Ga granitoid could be related to the amalgamation of an island arc to an Archean/Early Siderian block.

The 2.21, 2.18, 2.16–2.15, 2.13 Ga magmatic events are represented by the high-temperature deformed granitoids from the west part (Table 8). Besides different age ranges, these groups were distinguished by the difference in the abundance of high-temperature deformation (e.g. Vasquez et al., 2005), with high-temperature deformation being more common in the 2.21–2.18 Ga granitoids than in the 2.16–2.13 Ga granitoids. However, there are exceptions, demonstrated by the preservation of igneous textures in sample MVD27E and the high-temperature foliation in the sample MVD103A.

The features of high-temperature deformation in Rhyacian granitoids indicate an orogenic character for these granitoids. Thrusting features were not found because these rocks are strongly affected by the transcurrent shear zones that probably totally transposed thrusting structures.

The 2.21–2.18 Ga granitoids may be related to an early Rhyacian orogeny in the Bacajá domain and the 2.16–2.13 Ga granitoids could represent a late orogeny. Both orogenies are related to Trans-Amazonian cycle.

Detailed studies of Nd or Hf isotope data and geochesmistry are necessary to investigate the sources and setting of the Rhyacian granitoids, but the zircon geochronology and preliminary Nd isotope data allow outlining some interpretations.

Inherited zircon crystals of ca. 2.5 Ga were found in the granitoids of 2215 Ma (Vasquez et al., 2005) and 2182 Ma (Santos, 2003) from the Brasil Novo area, indicating Neoarchean crustal sources or a strong contamination. In addition, the 2133 Ma granitoid (sample MVD103A) has inherited zircon crystals of ca 2.34 Ga that indicate late Siderian crustal sources. On the other hand, Macambira et al. (2004) found in the Belo Monte area a granitoid of 2154 Ma with Nd isotope data (Table 1) with juvenile source. These points yield different sources for Rhyacian granitoids from the Bacajá domain, probably with dominant crustal component in the west part of the domain and a mixing with juvenile component of ca. 2.3 Ga (T_{DM}Nd) in the central to east part.

The predominance of tonalites and granodiorites with crustal contribution suggests that these granitoids could be magmatic arcs bordering the Neoarchean-Siderian craton (2.67–2.31 Ga crust). However, lithologic and tectonic associations as supracrustal rocks from basins related to these Rhyacian magmatic arcs were not found in the Bacajá domain.

The ca. 2.10 Ga magmatism is represented by granitoids and charnockitic rocks which sometimes show high-temperature deformation. They occur mainly in the west part and charnockitic bodies are associated with orthogranulites and paragneisses from the Terra do Meio area, whereas the granitoids (sample MVD102) usually are associated with other Rhyacian granitoids and the Três Palmeiras greenstone belt (Fig. 2). Vasquez et al. (2005) found inherited zircon crystals of 2.12–2.15 Ga in a granitoid of 2.10 Ga from the Uruará area, but these are absent in sample MVD102 suggesting a more limited contribution from older crustal sources. The thrusting tectonically juxtaposed granulites and charnockitic rocks with granitoids and supracrustal rocks, but the transcurrent shear zones obliterated the thrusting structures. The transcurrent tectonic regime seems to have strongly controlled the emplacement of the 2.10–2.07 Ga rocks.

Little evidence of continental collision was found in the Bacajá domain. Exhumation of granulites and associated charnockitic bodies by thrusting is the major consequence of collisional orogeny related to the 2.1 Ga collision of the Archean cratons in West Africa and northeastern South America (Feybesse and Milési, 1994; Ledru et al., 1994; Vanderhaeghe et al., 1998; Delor et al., 2003a). In this context, the granitoids and charnockitic rocks of ca. 2.10 Ga are related to a post-collisional magmatism, in the sense of Liégeois (1998), constrained to the

Table 4
Summary of SHRIMP U–Pb zircon data for sample MVD134A

Grains spot	^{206}Pb (%)	U (ppm)	Th (ppm)	^{232}Th/^{238}U	^{206}Pb* (ppm)	^{206}Pb/^{238}U age[a] (Ma)	^{207}Pb/^{206}Pb age[a] (Ma)	Percentage discordant	^{207}Pb*/^{206}Pb*[a]	± (%)	^{207}Pb*/^{235}U[a]	± (%)	^{206}Pb*/^{238}U[a]	± (%)	Errors correlation
1.1	0.02	144	45	0.32	55.2	2377 ± 19	2337 ± 7	−2	0.1493	0.44	9.177	1.05	0.4459	0.95	0.910
2.1	0.01	388	141	0.37	133	2157 ± 16	2327 ± 6	7	0.1484	0.37	8.130	0.93	0.3973	0.85	0.916
3.1	0.05	345	126	0.38	127	2295 ± 19	2327 ± 5	1	0.1484	0.30	8.750	1.01	0.4277	0.96	0.956
4.1	0.59	508	87	0.18	161	2008 ± 15	2302 ± 10	13	0.1462	0.60	7.367	1.04	0.3655	0.85	0.818
5.1	0.31	241	76	0.33	85.1	2211 ± 17	2328 ± 8	5	0.1484	0.49	8.375	1.02	0.4092	0.89	0.876
6.1	0.39	434	179	0.43	131	1938 ± 15	2270 ± 15	15	0.1435	0.86	6.941	1.22	0.3507	0.87	0.715
7.1	0.20	238	76	0.33	83.3	2198 ± 17	2310 ± 9	5	0.1469	0.52	8.226	1.07	0.4063	0.94	0.875
8.1	0.14	248	73	0.31	92.6	2324 ± 17	2333 ± 8	0	0.1488	0.47	8.908	1.00	0.4341	0.88	0.882
8.2	0.09	627	368	0.61	228	2269 ± 16	2334 ± 4	3	0.1490	0.24	8.664	0.87	0.4219	0.84	0.961
9.1	0.03	401	71	0.18	152	2360 ± 17	2327 ± 5	−1	0.1484	0.29	9.044	0.91	0.4421	0.86	0.949
9.2	0.00	233	71	0.31	87.9	2349 ± 21	2347 ± 6	0	0.1501	0.35	9.097	1.07	0.4396	1.05	0.948
10.1	0.81	210	62	0.30	70.5	2110 ± 17	2332 ± 15	10	0.1488	0.90	7.941	1.29	0.3871	0.93	0.717
10.2	0.15	573	180	0.33	152	1728 ± 13	2231 ± 6	23	0.1403	0.33	5.949	0.91	0.3075	0.84	0.932
11.1	0.09	174	52	0.31	56.1	2048 ± 16	2268 ± 12	10	0.1434	0.71	7.394	1.17	0.3740	0.94	0.798
11.2	0.02	194	76	0.40	72.8	2336 ± 18	2345 ± 6	0	0.1499	0.38	9.029	0.99	0.4367	0.91	0.923
12.1	0.01	180	57	0.33	69.9	2402 ± 19	2329 ± 7	−3	0.1486	0.41	9.248	1.03	0.4515	0.94	0.915
13.1	–	139	43	0.32	52.8	2366 ± 19	2346 ± 8	−1	0.1500	0.46	9.173	1.07	0.4434	0.97	0.903
14.1	0.12	598	51	0.09	130	1454 ± 11	2022 ± 7	28	0.1245	0.40	4.344	0.94	0.2530	0.85	0.903
15.1	0.36	167	50	0.31	56.7	2143 ± 18	2341 ± 13	8	0.1496	0.76	8.133	1.25	0.3944	1.00	0.794
16.1	0.06	221	79	0.37	83.3	2345 ± 22	2342 ± 7	0	0.1497	0.41	9.052	1.18	0.4387	1.11	0.939
17.1	0.14	168	57	0.35	61.8	2290 ± 19	2336 ± 9	2	0.1492	0.54	8.772	1.13	0.4265	0.99	0.877
17.2	0.05	310	128	0.42	81.8	1725 ± 14	2240 ± 7	23	0.1411	0.42	5.967	1.00	0.3068	0.90	0.906
18.1	0.03	225	62	0.28	85.5	2360 ± 19	2325 ± 7	−1	0.1482	0.40	9.034	1.04	0.4421	0.96	0.923

Errors are 1σ; Pb* indicate the radiogenic portion. Error in standard calibration was 0.25% (not included in above errors but required when comparing data from different mounts).
[a] Common Pb corrected using measured ^{204}Pb.

Table 5
Summary of SHRIMP U–Pb zircon data for sample MVD125A

Grains spot	^{206}Pb (%)	U (ppm)	Th (ppm)	^{232}Th/^{238}U	^{206}Pb* (ppm)	^{206}Pb/^{238}U age[a] (Ma)	^{207}Pb/^{206}Pb age[a] (Ma)	Percentage discordant	^{207}Pb*/^{206}Pb*[a]	± (%)	^{207}Pb*/^{235}U[a]	± (%)	^{206}Pb*/^{238}U[a]	± (%)	Errors correlation
1.1	0.13	426	173	0.42	143	2126 ± 19	2165 ± 7	2	0.1351	0.40	7.276	1.13	0.3906	1.06	0.934
2.1	0.12	4162	4605	1.14	850	1374 ± 13	2049 ± 29	33	0.1264	1.61	4.140	1.93	0.2375	1.02	0.530
2.2	0.07	929	639	0.71	316	2149 ± 19	2163 ± 4	1	0.1349	0.26	7.361	1.06	0.3957	1.03	0.971
3.1	0.10	512	191	0.39	170	2109 ± 18	2165 ± 6	3	0.1351	0.35	7.207	1.04	0.3869	0.99	0.943
4.1	0.08	511	203	0.41	175	2163 ± 18	2149 ± 6	−1	0.1338	0.34	7.354	1.05	0.3986	0.99	0.945
5.1	0.30	333	137	0.42	115	2176 ± 20	2155 ± 9	−1	0.1343	0.55	7.437	1.23	0.4016	1.11	0.896
5.2	0.22	1248	1013	0.84	364	1879 ± 24	2115 ± 12	11	0.1313	0.67	6.124	1.63	0.3383	1.49	0.912
6.1	0.05	665	402	0.62	204	1964 ± 17	2139 ± 6	8	0.1331	0.35	6.537	1.04	0.3561	0.98	0.943
6.2	0.14	262	113	0.44	92.8	2222 ± 20	2156 ± 10	−3	0.1344	0.59	7.626	1.23	0.4115	1.08	0.876
7.1	0.03	411	193	0.48	136	2102 ± 18	2158 ± 6	3	0.1346	0.37	7.154	1.08	0.3856	1.01	0.938
8.1	0.03	523	264	0.52	172	2093 ± 18	2159 ± 9	3	0.1346	0.33	7.120	1.05	0.3837	0.99	0.949
9.1	0.00	559	255	0.47	185	2106 ± 18	2161 ± 6	3	0.1348	0.32	7.180	1.04	0.3864	0.99	0.950
10.1	–	362	133	0.38	120	2106 ± 19	2167 ± 7	3	0.1349	0.40	7.185	1.10	0.3863	1.03	0.933
11.1	0.02	506	193	0.39	168	2105 ± 18	2154 ± 6	2	0.1342	0.34	7.146	1.05	0.3862	1.00	0.947
12.1	–	699	532	0.79	233	2115 ± 18	2169 ± 5	2	0.1354	0.28	7.247	1.01	0.3883	0.97	0.961
12.2	0.02	395	257	0.67	131	2099 ± 18	2156 ± 7	3	0.1344	0.39	7.129	1.09	0.3848	1.02	0.935
13.1	0.38	362	140	0.40	127	2204 ± 19	2164 ± 14	−2	0.1350	0.78	7.591	1.29	0.4077	1.03	0.800
14.1	0.00	582	239	0.42	192	2099 ± 18	2160 ± 5	3	0.1347	0.31	7.150	1.04	0.3849	0.99	0.953

Errors are 1σ; Pb* indicate the radiogenic portions. Error in standard calibration was 0.44% (not included in above errors but required when comparing data from different mounts). [a] Common Pb corrected using measured ^{204}Pb.

Table 6
Summary of SHRIMP U–Pb zircon data for sample MVD115B

Grains spot	^{206}Pb (%)	U (ppm)	Th (ppm)	^{232}Th/^{238}U	^{206}Pb* (ppm)	^{206}Pb/^{238}U age[a] (Ma)	^{207}Pb/^{206}Pb age[a] (Ma)	Percentage discordant	^{207}Pb*/^{206}Pb*[a]	± (%)	^{207}Pb*/^{235}U[a]	± (%)	^{206}Pb*/^{238}U[a]	± (%)	Errors correlation
1.1	0.25	335	140	0.43	106	2014 ± 20	2166 ± 11	7	0.1352	0.62	6.835	1.30	0.3667	1.14	0.878
2.1	0.24	337	181	0.55	92	1776 ± 18	2148 ± 11	17	0.1337	0.62	5.848	1.30	0.3171	1.14	0.880
2.2	2.06	45	14	0.32	6.6	1002 ± 18	2242 ± 75	55	0.1412	4.34	3.274	4.75	0.1681	1.95	0.410
3.1	0.28	164	94	0.59	50.2	1956 ± 21	2161 ± 14	9	0.1348	0.83	6.586	1.51	0.3544	1.26	0.834
4.1	0.47	185	133	0.74	60.4	2067 ± 22	2148 ± 16	4	0.1338	0.93	6.972	1.55	0.3779	1.24	0.800
5.1	0.00	363	131	0.37	125	2179 ± 21	2152 ± 7	−1	0.1341	0.43	7.435	1.21	0.4023	1.13	0.935
6.1	0.00	268	153	0.59	91.9	2167 ± 22	2150 ± 12	−1	0.1339	0.67	7.378	1.35	0.3997	1.17	0.869
7.1	0.34	113	56	0.51	30.5	1751 ± 21	2151 ± 19	19	0.1340	1.11	5.767	1.76	0.3122	1.37	0.777
8.1	0.04	432	165	0.40	146	2139 ± 20	2136 ± 7	0	0.1328	0.40	7.206	1.18	0.3935	1.11	0.939
9.1	1.07	316	120	0.39	102	2035 ± 20	2152 ± 24	5	0.1341	1.35	6.864	1.78	0.3713	1.16	0.650
10.1	0.02	99	72	0.75	34	2171 ± 26	2171 ± 15	0	0.1355	0.86	7.485	1.65	0.4005	1.41	0.854
11.1	0.02	479	48	0.10	164	2167 ± 20	2149 ± 6	−1	0.1338	0.37	7.378	1.16	0.3997	1.10	0.948
12.1	1.00	247	126	0.53	84.2	2135 ± 22	2128 ± 28	0	0.1323	1.60	7.160	1.99	0.3926	1.19	0.596
12.2	0.07	83	58	0.73	29.2	2215 ± 28	2137 ± 16	−4	0.1329	0.93	7.513	1.74	0.4100	1.48	0.846
13.1	0.03	406	150	0.38	140	2176 ± 21	2141 ± 7	−2	0.1332	0.41	7.378	1.19	0.4016	1.12	0.938
15.1	0.03	158	101	0.66	55	2192 ± 24	2155 ± 12	−2	0.1343	0.67	7.501	1.45	0.4050	1.28	0.886
16.1	4.09	112	64	0.59	39.9	2154 ± 26	2153 ± 83	0	0.1341	4.74	7.335	4.95	0.3967	1.42	0.288
17.1	0.00	49	46	0.98	16.4	2122 ± 30	2112 ± 31	0	0.1310	1.75	7.044	2.40	0.3899	1.64	0.683
17.2	0.16	295	139	0.49	93.2	2018 ± 21	2146 ± 16	6	0.1336	0.90	6.772	1.49	0.3676	1.19	0.798

Errors are 1σ; Pb* indicate the radiogenic portion. Error in standard calibration was 0.35% (not included in above errors but required when comparing data from different mounts).
[a] Common Pb corrected using measured ^{204}Pb.

NW–SE transcurrent shear zones, emplaced under transpressive to transtractive conditions.

The 2.08–2.07 Ga magmatism comprises granitoids and charnockitic rocks with preserved igneous textures or affected by low-temperature deformation related to the late-stage NW–SE transcurrent shear zones, where they are the post-transcurrent granitoids. The large volume of 2.08–2.07 Ga granites as well as the occurrence of inherited zircon crystals of 2.22–2.09 Ga in the 2.08 Ga granites from west part of the Bacajá domain (Vasquez et al., 2005) and the Nd isotope data (T_{DM} ca. 2.6 Ga and $\varepsilon Nd_{(t)}$ of −4.25, Macambira et al., 2004) for these granites from the east part indicate a significant crustal participation in their source. On the other hand, the intermediate charnockitic rocks of 2.07 Ga (sample MVD94) have a juvenile source or minor crustal contamination and these rocks can be related to underplating of mafic magmas and upwelling of mantle.

A younger magmatic event of 1.99 Ga was found by Vasquez et al. (2005) in the northwestern part of the study area. It is represented by a granitoid pluton intruded into high-grade rocks and Rhyacian granitoids (Fig. 2). This magmatism could be related to the end of the Trans-Amazonian cycle. However, there is high-K calc-alkaline magmatism of 2.0–1.96 Ga related to evolution of the Orosirian orogeny of the adjacent Ventuari-Tapajós or Parima-Tapajós province (Lamarão et al., 2002; Vasquez et al., 2002; Santos et al., 2004). Therefore, this granitoid pluton of 1.99 Ga may be a local occurrence of the 2.0–1.96 Ga magmatism, suggesting that this event extended to the foreland.

5.2. Archean and paleoproterozoic scenarios in amazonian craton

The Trans-Amazonian domains of the northeastern Guiana shield contain few remnants of Archean crust. They are constrained by detrital and inherited zircon ages and by Nd isotope data of metasedimentary rocks of the Rhyacian greenstone belts and granitoids (Delor et al., 2003a). In the southeastern Guiana shield, the evidence for Archean rocks is more substantial, with occurrences of inherited zircon (2.78–2.59 Ga), Nd isotope data (T_{DM} = 2.68–2.5 Ga) and Neoarchean inliers (ca. 2.6 Ga) within Rhyacian (2.19–2.07 Ga) granitoids and charnockitic rocks from Paleoproterozoic domains and widespread reworked Archean (3.3–2.6 Ga) basement from Amapá block (Pimentel et al., 2002; Ricci et al., 2002; Avelar et al., 2003; Klein et al., 2003; Rosa-Costa et al., 2003, 2006). Late Neoarchean to Siderian rocks (2.58–2.36 Ga) have been identified in the Amapá block

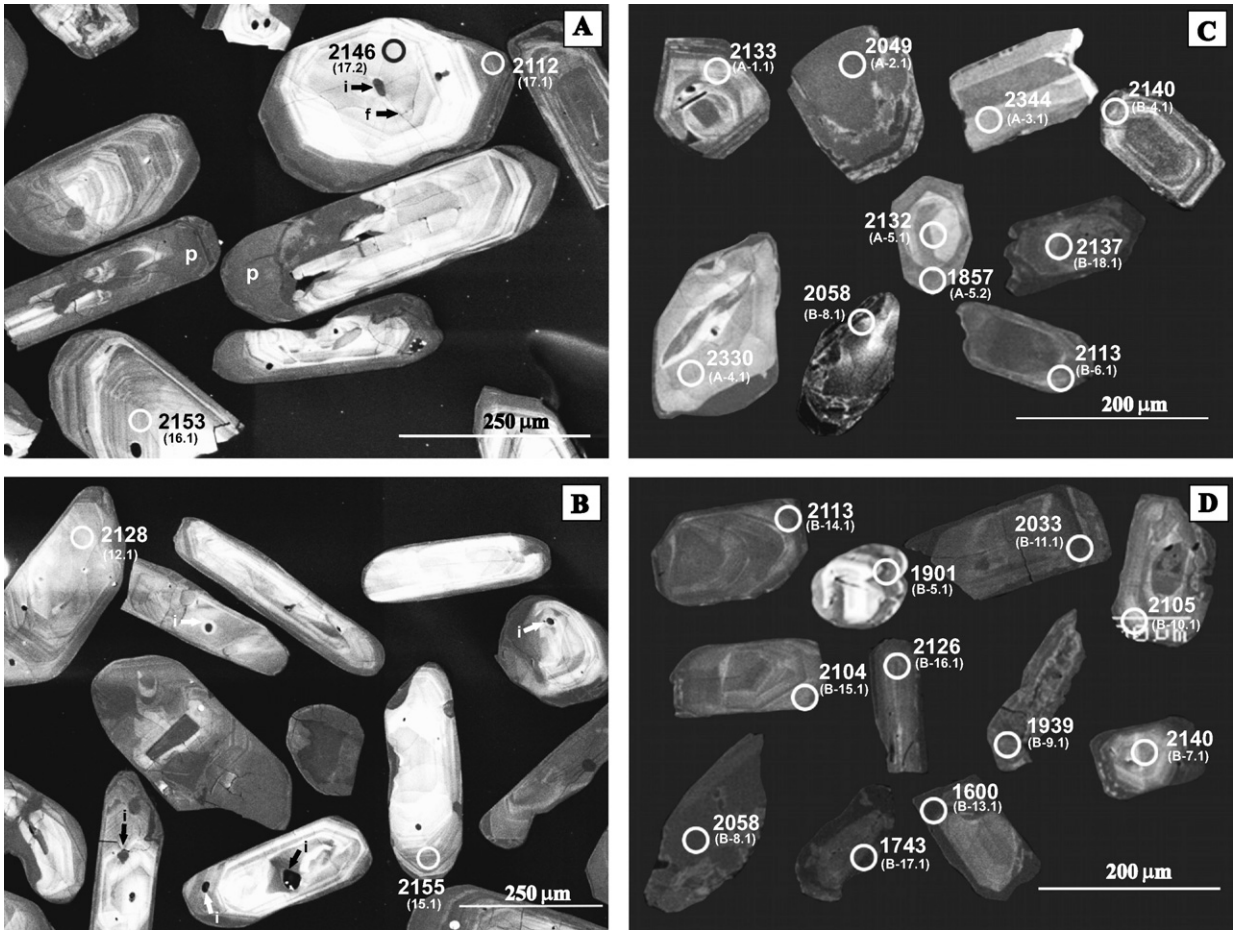

Fig. 7. Cathodoluminescence images of analyzed zircon crystals of the samples MVD115B (A and B) and MVD103A (C and D), with the ion microprobe spots, their number in the parentheses and their respective $^{207}Pb/^{206}Pb$ ages. Detail of metamict patches (p) mineral inclusions (i) and radial microfractures (f) of zircon crystals (A and B) of the sample MVD115B.

Table 7
Summary of SHRIMP U–Pb zircon data for sample MVD103A

Grains spot	^{206}Pb (%)	U (ppm)	Th (ppm)	^{232}Th/^{238}U	^{206}Pb* (ppm)	^{206}Pb/^{238}U age[a] (Ma)	^{207}Pb/^{206}Pb age[a] (Ma)	Percentage discordant	^{207}Pb*/^{206}Pb*[a]	± (%)	^{207}Pb*/^{235}U[a]	± (%)	^{206}Pb*/^{238}U[a]	± (%)	Errors correlation
A-1.1	0.04	193	85	0.45	67.1	2185 ± 29	2133 ± 8	−2	0.1326	0.43	7.376	1.64	0.4035	1.58	0.965
A-2.1	0.01	463	17	0.04	147	2021 ± 15	2049 ± 5	1	0.1264	0.29	6.418	0.90	0.3682	0.85	0.948
A-3.1	0.01	143	45	0.33	54.4	2366 ± 23	2344 ± 8	−1	0.1498	0.45	9.163	1.26	0.4435	1.18	0.935
A-4.1	0.01	157	38	0.25	59.3	2351 ± 18	2330 ± 8	−1	0.1486	0.46	9.019	1.02	0.4400	0.91	0.894
A-5.1	0.07	114	103	0.93	38.0	2112 ± 20	2132 ± 17	1	0.1325	0.98	7.083	1.48	0.3877	1.11	0.751
A-5.2	7.21	825	940	1.18	234	1721 ± 15	1857 ± 140	7	0.1136	7.94	4.789	8.01	0.3059	1.00	0.125
B-2.1	0.97	129	95	0.77	22.8	1197 ± 19	1294 ± 63	7	0.0840	3.22	2.365	3.67	0.2041	1.77	0.481
B-3.1	–	270	46	0.18	86.0	2036 ± 41	2357 ± 18	14	0.1510	1.05	7.730	2.57	0.3713	2.35	0.912
B-4.1	–	176	67	0.39	58.6	2108 ± 29	2140 ± 10	2	0.1332	0.57	7.104	1.73	0.3868	1.63	0.944
B-5.1	1.58	618	143	0.24	97.4	1070 ± 17	1901 ± 42	44	0.1302	1.35	2.896	2.88	0.1806	1.69	0.588
B-6.1	–	267	102	0.40	83.1	1995 ± 28	2113 ± 10	6	0.1311	0.59	6.558	1.74	0.3627	1.63	0.941
B-7.1	–	154	104	0.70	50.7	2092 ± 33	2140 ± 11	2	0.1332	0.62	7.038	1.97	0.3833	1.87	0.950
B-8.1	0.00	1733	2537	1.51	544	2006 ± 27	2058 ± 3	3	0.1271	0.19	6.398	1.57	0.3651	1.56	0.993
B-9.1	1.99	2639	124	0.05	483	1223 ± 21	1939 ± 38	37	0.1363	0.20	3.423	2.84	0.2088	1.89	0.667
B-10.1	0.00	256	94	0.38	71.8	1824 ± 26	2105 ± 11	13	0.1306	0.64	5.886	1.74	0.3270	1.62	0.931
B-11.1	0.00	782	128	0.17	205	1719 ± 29	2033 ± 12	15	0.1253	0.69	5.280	2.01	0.3057	1.89	0.940
B-12.1	0.00	355	27	0.08	28.4	577 ± 9	509 ± 25	−13	0.0574	1.16	0.738	2.01	0.0931	1.64	0.818
B-13.1	0.11	2681	117	0.05	428	1098 ± 27	1600 ± 190	31	0.0987	9.94	2.529	10.41	0.1858	2.71	0.260
B-14.1	0.02	358	134	0.39	105	1900 ± 29	2113 ± 7	10	0.1311	0.41	6.199	1.81	0.3428	1.77	0.974
B-15.1	0.01	278	135	0.50	86.3	1987 ± 29	2104 ± 7	6	0.1304	0.42	6.492	1.72	0.3610	1.67	0.970
B-16.1	0.01	209	131	0.65	71.1	2150 ± 30	2126 ± 8	−1	0.1321	0.47	7.211	1.70	0.3958	1.62	0.960
B-17.1	0.06	1239	114	0.09	173	971 ± 35	1743 ± 11	44	0.1066	0.59	2.390	3.92	0.1625	3.88	0.988
B-18.1	0.01	360	193	0.56	113	2010 ± 28	2137 ± 7	6	0.1329	0.38	6.707	1.66	0.3660	1.6	0.974

Errors are 1σ; Pb* indicate the radiogenic portion. Errors in standard calibrations were 0.25% and 1.29% for analyses from mount A and B, respectively.
[a] Common Pb corrected using measured ^{204}Pb.

Table 8
Magmatic events from the Bacajá domain

Period[a]	Zircon age	Rocks/events	Setting
Neoarchean (2850–2500 Ma)	2671 Ma (1) 2503–2487 Ma (2, 3) 2452–2440 Ma (3, 4)	Orthogneisses and felsic metavolcanoclastic rocks related to Neoarchean to early Siderian magmatic events	2.67 Ga juvenile crust (island arc?) and 2.5–2.44 Ga crust with crustal component (active margin?)
Siderian (2500–2300 Ma)	2359 Ma (1), 2338 Ma (3) 2313 Ma (5)	Mafic to intermediate metavolcanic rocks and metagranitoids related to Late Siderian magmatic events	2.36–2.34 Ga island-arc and 2.31 Ga granitoid related to late stage of amalgamation of an island arc to an Archean block
	2215–2209 Ma (3, 4) 2182 Ma (2)	Early Rhyacian granitoids related to the early orogenic interval of the Trans-Amazonian cycle	2.21–2.18 Ga magmatic arcs (active margin) bordering Neoarchean to Siderian craton
	2160 Ma (3), 2154 Ma (6) 2147 Ma (3), 2133 Ma (3)	Middle Rhyacian granitoids related to the main orogenic interval of the Trans-Amazonian cycle	2.16–2.13 Ga magmatic arcs (active margin)
Rhyacian (2300–2050 Ma)	2114 Ma (5) 2104–2102 Ma (3, 4) 2086 Ma (2)	Late Rhyacian granitoids and charnockitic rocks related to main Trans-Amazonian collision	2.11 Ga collisional (?) and 2.10–2.09 Ga early post-collisional (continental collision)
	2077–2069 Ma (3, 4, 6, 7)	Late Rhyacian granitoids and charnockitic rocks related to post-collisional stage of the Trans-Amazonian collision	2.08–2.07 Ga late post-collional (post-orogenic)
Orosirian (2050–1800 Ma)	1986 Ma (4)	Orosirian granitoid, probably not related to Trans-Amazonian cycle. Perhaps a foreland magmatic pulse of an Orosirian orogenic magmatism	1.99 Ga post-orogenic to anorogenic

Key to references: (1) Macambira et al. (2004); (2) Santos (2003); (3) this work; (4) Vasquez et al. (2005); (5) Faraco et al. (2005); (6) Macambira et al. (2003) and (7) Souza et al. (2003).
[a] Subdivision of the Precambrian recommended by International Union of Geological Sciences, Plumb (1991).

(Rosa-Costa et al., 2006) and remnants enclosed in Trans-Amazonian domains have been interpreted as mixtures between Proterozoic juvenile sources and Archean reworked sources, rather than new formation of Siderian crust (Avelar et al., 2003; Rosa-Costa et al., 2006). However, juvenile accretion at 2.3 Ga related to an early orogenic phase is suggested by Nd isotope data (T_{DM} of 2.32 Ga and $\varepsilon Nd_{(t)}$ of + 1.17) for an orthogneiss of a Trans-Amazonian domain (Rosa-Costa et al., 2006).

Neoarchean and early Siderian remnants are frequent in the Bacajá domain, but until now the full extent of reworked Archean basement has not been known. The 2.67, 2.50 and 2.45 Ga rocks are the oldest rocks from this domain.

The occurrence of probable juvenile 2.36–2.34 Ga rocks in this domain indicates a late Siderian event of crust formation. The existence of Siderian crust in the Amazonian craton is reinforced by the occurrence of detrital zircon populations of ca. 2.35 and 2.44 Ga, respectively, found in the sandstones from foreland basins of the northernmost (Roraima Supergroup) and the southeastern (Castelo dos Sonhos Formation) Central Amazonian province (Santos, 2003; Santos et al., 2003b).

According to the crustal evolution model based on Nd isotope data proposed by Cordani and Sato (1999), the South America Platform did not show significant growth and recycling of continental crust during the period between 2.5 and 2.3 Ga. There are records which suggest formation of Siderian crust in the São Francisco craton; they are related to a Siderian taphrogenesis that preceded Trans-Amazonian orogenies (Delgado et al., 2003). These authors refer to mantle-derived intraplate magmatic events with shoshonitic, mangeritic and mafic–ultramafic rocks for which Rb–Sr, Pb–Pb and Sm–Nd data furnished ages between 2.6 and 2.4 Ga. During this period the continental platform sediments and BIFs were deposited in the passive margin basin from Quadrilátero Ferrífero region (Alkimim and Marshak, 1998). In addition, other records such as a 2.47 Ga granite related to 2.85–2.63 Ga granulite complexes from the Jequié block (Silva et al., 2002) and a 2.36 Ga juvenile granite ($\varepsilon Nd_{(t)}$ of + 0.13) from southwestern Quadrilátero Ferrífero region (Endo and Machado, 2002, and references therein) further support the existence of Siderian crust. Other expressive occurrences of Siderian rocks in the South America are the 2.29–2.36 Ga orthogneisses from the NW Ceará domain of the Borborema province in northeastern Brazil; Nd isotope data for most rocks this domain indicate a juvenile crust probably related to an island-arc (Fetter et al., 2000). In the southern Brazilian shield, Hartman et al. (2004) found detrital zircon populations of 2.47 and 2.35 Ga with magmatic Th–U ratio in quartzites from the Porongos Complex, which probably came from granitoids of these ages found further to the west.

Four Rhyacian orogenies between 2264 and 2011 Ma of the Trans-Amazonian cycle were distinguished in the Rio de La Plata craton and associated belts, as well as in other Trans-Amazonian terranes from northern South America (Santos et al., 2003a). The oldest orogeny (2264–2201 Ma) is related to

Table 9
Magmatic and metamorphic events of the Trans-Amazonian segments from the Amazonian craton

Bacajá domain	Carecuru domain	Paru domain	Amapá block	French Guiana domain	Bakhuis belt
2.21–2.18 Ga granitoids, early orogenic interval, older magmatic arcs, continental active margin	2.19–2.18 Ga calc-alkaline granitoids, magmatic arc-older pulse of accretion stage (1)		2.21 and 2.18 Ga granitoids, early orogenic phase, crustal reworking (1, 2)	2.22–2.21 Ga gabbros - oceanic stage (5)	
				2.18–2.16 Ga TTG granitoids relate to older magmatic arc (5)	
2.16–2.13 Ga granitoids, main orogenic interval, younger magmatic arcs, continental active margin	2.15–2.14 Ga calc-alkaline granitoids, magmatic arc, younger pulse of accretion stage (1)		2.15 Ga leucogranite - crustal reworking (1, 2)	2.15–2.13 Ga TTG granitoids - younger magmatic arc (5)	
2.10 Ga granitoids, early post-collisional phase of the Trans-Amazonian collision	2.10 Ga granites, reworking of calc-alkaline granitoids (1)			2.11–2.08 Ga pyroxene granitoids and gabbros – sliding/docking and migmatization of TTG granitoids (5)	
			2.09 Ga leucosome of granulites - oblique thrusting, granulite metamorphism, collisional stage (2)		
2.08–2.07 Ga granitoids, transcurrent shearing, late post-collisional phase				2.07–2.06 Ga granites relate to strike slip shearing - crustal stretching (5)	
2.07 Ga charnonockitic rocks relate to late post-collisional phase		2.07 Ga charnockitic rocks - late post-collisional stage (1)	2.06–2.05 charnockitic rocks, late post-collisional stage (3)		2.07–2.05 Ga charnockitic rocks, pegmatites and mafic dykes and coeval UHT metamorphism, crustal stretching, mantle upwelling and lower crust exhumation (6, 7)
			2.03–2.0 Ga granulite metamorphism (3, 4) 2.05–2.03 Ga granites and 2.06–2.04 Ga leucosome of orthogneiss - strike slip shearing - late orogenic stage (1, 2)		
1.99 Ga granitoid, a post- orogenic phase of the Trans-Aamzonian cycle or foreland pulse of the 2.0–1.96 Ga orogenic magmatism					1.98 Ga anorthosite, late magmatic pulse of the 2.06 mafic magmatism (6)

Key to references: (1) Rosa-Costa et al. (2006); (2) Rosa-Costa et al. (in press); (3) Lafon et al. (2001); (4) Oliveira (2002); (5) Delor et al. (2003a); (6) Roever et al. (2003); (7) Delor et al. (2003b).

island-arcs; a second, 2180–2120 Ma, is composed of syn- to late-orogenic granitoids and greenstone belt sequences; a third orogeny of 2080–2050 Ma, is mostly represented by late to post-orogenic granitoids and charnockitic rocks with associated high-grade metamorphism, and the youngest orogeny (2020–2011 Ma) is marked by minor granitic magmatism and intense hydrothermal events. The three first orogenies are present in the Bacajá domain. The early and main Trans-Amazonian orogenic associations are respectively represented by granitoids of 2.21–2.18 and 2.16–2.13 Ga (Table 9), but until now their coeval greenstone belts remain unknown. The granitoid-greenstone association in this domain is 2.36–2.34 Ga, being older (80–100 Ma) than those related to the early orogenic interval of the Trans-Amazonian cycle.

Similar age ranges have been found in the southeastern Guiana shield, where Rosa-Costa et al. (2006) distinguished calc-alkaline granitoids of 2.19–2.18 and 2.15–2.14 Ga in the Carecuru domain and 2.22–2.18 Ga granitoids in the Amapá block (Table 9). In northeastern Guiana shield, some TTG associations and Gabbros related to oceanic stage provided zircon ages between 2.21 and 2.22 Ga, whereas the 2.18–2.16 and 2.15–2.13 Ga granitoids, related to two successive magmatic arcs, are progressively younger to the central domain (Delor et al., 2003a).

The ca. 2.10 Ga magmatism of the Bacajá domain are related to an early post-collisional stage. Some granitoids of this period preserve a magmatic arc signature, with predominance of hornblende-bearing granodiorites and tonalites typical of calc-alkaline associations, but their close relationship with high-temperature deformed charnockitic rocks and associated granulites suggests a thrusting tectonic scenario related to a collision event followed by transcurrent tectonic typical of intra-continental setting. This inherited magmatic arc signature has been described in many post-collisional associations as being a result of sources of rock and not just geodynamic setting (Harris et al., 1986; Sylvester, 1989; Förster et al., 1997; Pearce, 1996; Liégeois et al., 1998).

Intrusion relationship in Uruará area (Fig. 2) indicate that high-temperature deformed charnockitic rocks are slight older than the 2.10 Ga granitoids. Probably, these early charnockitic rocks are related to the initial major impact (syn-collision).

Similar post-collisional associations are found in other Trans-Amazonian domains of the Amazonian craton. In the northeastern Guiana shield (Table 9), this event is represented by the emplacement of 2.11–2.08 Ga granitoids and pyroxene-bearing granites along sinistral transcurrent shear zones, opening of detrital basins and reworking (migmatization) of TTG associations (Delor et al., 2003a). Post-collisional magmatism, associated metamorphism and sedimentation of pull-apart basins reflect the docking and sliding of the African and South American plates during the 2.1 Ga collision event (Feybesse and Milési, 1994; Ledru et al., 1994; Vanderhaeghe et al., 1998; Delor et al., 2003a,b). To the southeast, migmatization and granulite facies metamorphism at 2.09 Ga, related to thrust tectonics of the 2.1 Ga collision, have been found in the Archean orthogneisses from the Amapá block (Rosa-Costa et al., in press). Additionally, 2.10 Ga granites related to reworking of calc-alkaline granitoids have been found in the Carecuru Domain (Rosa-Costa et al., 2006).

The evolution of the post-collisional scenario in the Bacajá domain was also marked by the emplacement of 2.08–2.07 Ga granitoids and charnockitic rocks. These bodies are usually strongly controlled by transcurrent shear zones (Fig. 2) and have evolved compositions, significant crustal sources (except for intermediate to mafic charnockitic rocks), further supporting the intraplate character typical of post-collisional associations. Analogies with other Trans-Amazonian domains of the Guiana shield are possible (Table 9). Delor et al. (2003b) and Rover et al. (2003) described dextral shearing with emplacement of metaluminous granites of 2.07–2.06 Ga, ultrahigh-temperature granulite facies metamorphism with associated 2.07–2.05 Ga charnockite plutons, mafic dykes and pegmatite veins during this stage in the northeastern and northern Guiana shield. According to these authors, these post-collisional associations are related to a crustal stretching event which was followed by exhumation of the lower crust rocks by normal faults and burial metamorphism of pull-apart basins. Coeval charnockitic magmatism and granulite metamorphism have been found in the southern and southeastern Guiana shield (Lafon et al., 2001; Oliveira, 2002; Rosa-Costa et al., in press). This granulite metamorphism and associated charnockitic magmatism seems to be common in the Trans-Amazonian domains from Amazonian craton, as well as other Trans-Amazonian domains in South America (Santos et al., 2003a).

There timing of the last event of the Trans-Amazonian cycle is controversial. Some authors restrict it to ca. 2.0 Ga (Santos et al., 2000, 2003a; Nomade et al., 2002). In the northeastern part of the Guiana shield, Roever et al. (2003) identified a thermal event of ca. 2.0 Ga based on a U–Th–Pb date for a monazite from a leucogranite, which correspond to a magmatic pulse of 1.98 Ga. On the other hand, the 2.05–2.03 Ga granites from Amapá block are the latest magmatic pulses of the Trans-Amazonian cycle found in the southern Guiana shield (Table 9). Therefore, the tonalite pluton of 1.99 Ga may be the youngest magmatism of the post-orogenic stage of the Trans-Amazonian orogenies in the Bacajá domain. However, there is a gap of ca. 70 Ma between this event and the previous magmatic event. Alternatively, this tonalite could represent a local magmatic pulse of the Orosirian event between 2.0 and 1.96 Ga and related to the evolution of the adjacent Ventuari-Tapajós province, as previously discussed. This event is widespread from the southern to northern parts of this geochronological province, and local occurrences of these bodies could be found in the foreland, to the east of this orogenic belt. Due to the scarcity of mapped occurrences and other data about the rocks of ca. 1.99 Ga in the study area, as well as the uncertain position of this event regarding to Trans-Amazonian orogenies, the 2.08–2.07 Ga magmatism is preliminarily considered, in this work, to be the last magmatic event of the post-collisional stage of the Trans-Amazonian cycle in the west part.

6. Conclusions

Zircon geochronology has made it possible to identify and document Neoarchean (2.67 Ga), early Siderian (2.50 and

2.45 Ga), and late Siderian (2.36–2.34 Ga) magmatic events, as well as six Rhyacian (2.21; 2.18; 2.16–2.15; 2.13; 2.10–2.09 and 2.08–2.07 Ga) magmatic events in the western Bacajá domain.

The early Siderian magmatic events are represented by orthogneisses and remnants of supracrustal rocks. These orthogneisses have inherited cores and zircon crystals which suggested the existence of an old crustal component in the region. There is older orthogneiss of ca. 2.67 Ga from juvenile, but in several aspects these Neoarchean to early Siderian rocks from the Bacajá domain differ with those of the Carajás province.

The late Siderian magmatism seems to be related to amalgamation of an island arc, as indicated by the granitoid-greenstone belt of the Três Palmeiras area (2.36–2.34 Ga), to an Archean crustal block. Late Siderian igneous rocks are rare within the South American plate. In the Guiana shield, Siderian ages have been only recorded through Nd isotopes and detrital zircon. Therefore, occurrence of Siderian rocks distinguishes the Bacajá domain from other Trans-Amazonian domains in the Amazonian craton.

The Rhyacian magmatic events have similar age range to those found in the Trans-Amazonian domains of South America, especially those of the Guiana shield. In the evolution of the Trans-Amazonian cycle, the events between 2.21 and 2.13 Ga are related to magmatic arcs, whereas the ca. 2.10 Ga magmatism is related to the beginning of the post-collision stage marked by crustal thickening and movement along shear zones. The latest step was marked by 2.08–2.07 Ga magmatism and granulite facies metamorphism, which are related to reactivations of transcurrent shear zones and crustal stretching as proposed for the northern Guiana shield (Vanderhaeghe et al., 1998; Delor et al., 2003a,b).

Finally, there is uncertainty about the magmatic event of 1.99 Ga found in the study area (Vasquez et al., 2005), and whether it is magmatic pulse which can be related to the Trans-Amazonian cycle. If not, the 2.08–2.07 Ga may be the youngest Trans-Amazonian magmatic event in the Bacajá domain.

Acknowledgments

This work was supported by CPRM, Geological Survey of Brazil, projects PRONEX/CNPq 103/98 (grant 662103/1998-0), CNPq (grant 467104/00-0) and CT-Mineral/FINEP 01/2001. Marco Antonio Galarza and Rosemary Brabo are acknowledged for technical support during analytical work at UFPA, as well as Chuck Magee (ANU).The SHRIMP analyses were carried out during doctoral stage of the first author at ANU, which the scholarship was supported by CAPES Foundation (grant BEX 3310/04-3). This article is a contribution to PRONEX/CNPq 103/98.

References

Alkimim, F.F., Marshak, S., 1998. Transamazonian orogeny in the southern São Francisco Craton region, Minas Gerais, Brazil: evidence for Paleoproterozoic collision and collapse in the Quadrilátero Ferrífero. Precam. Res. 90, 29–58.

Avelar, V.G., Lafon, J.M., Delor, C., Guerrot, C., Lahondère, D., 2003. Archean crustal remnants in the easternmost part of the Guiana Shield: Pb–Pb and Sm–Nd geochronological evidence for Mesoarchean versus Neoarchean signatures. Geologie de la France 2–4, 83–100.

Barros, C.E.M., Macambira, M.J.B., Barbey, P., Scheller, T., 2004. Dados isotópicos Pb-Pb em zircão (evaporação) e Sm–Nd do Complexo Granítico Estrela, Província Mineral de Carajás Brasil: implicações petrológicas e tectônicas. Revista Brasil. Geociências 34 (4), 531–538.

Bertrand, J.M., Jardim de Sá, E.F., 1990. Where are the Erbunean-Transamazonian collisional belts? Can. J. Earth Sci. 27, 1382–1393.

Claoue-Long, J.C., Compston, W., Roberts, J., Fanning, C.M., 1995. Two Carboniferous ages: a comparison of SHRIMP zircon dating with conventional zircon ages and $^{40}Ar/^{39}Ar$ analysis. In: Berggren, W.A., Kent, D.V., Aubry, M.-P., Ardenbol, J. (Eds.), Geochronology, Time Scale and Global Stratigraphic Correlation, 4. Society for Sedimentary Geology, Special Publication, pp. 3–21.

Compston, W., Williams, I.S., Meyer, C., 1984. U–Pb geochronology of zircons from lunar breccia 73217 using a sensitive high-resolution ion-microprobe. J. Geophys. Res. B 98, 525–534.

Cordani, U.G., Sato, K., 1999. Crustal evolution of the South American Platform, based on Nd isotopic systematics on granitoid rocks. Episodes 22, 67–173.

Cordani, U.G., Tassinari, C.C.G., Kawashita, K., 1984. A Serra dos Carajás como região limítrofe entre províncias tectônicas. Ciências da Terra 9, 6–11.

Cordani, U.G., Tassinari, C.C.G., Teixeira, W., Basei, M.A.S., Kawashita, K., 1979. Evolução tectônica da Amazônia com base nos dados geocronológicos. Congress. Geol. Chileno, 2, Arica, Chile, Actas 4, 137–148.

Dall'Agnol, R., Costi, H.T., Leite, A.A.S., Magalhães, M.S., Texeira, N.P., 1999a. Rapakivi granites from Brazil and adjacent areas. Precam. Res. 95, 9–39.

Dall'Agnol, R., Rämö, O.T., Magalhães, M.S., Macambira, M.J.B., 1999b. Petrology of the anorogenic, oxidised Jamon and Musa granites Amazonian Craton: implications for the genesis of Proterozoic A-type granites. Lithos 46, 431–462.

Delgado, I.M., Souza, J.D., Silva, L.C., Silveira Filho, N.C., Santos, R.A., Pedreira, A.J., Guimarães, J.T., Angelim, L.A.A., Vasconcelos, A.M., Gomes, I.P., Lacerda Filho, J.V., Valente, C.R., Perrota, M.M., Heineck, C.A., 2003. Geotectônica do Escudo Atlântico. In: Bizzi, L.A., Schobbenhaus, C., Vidotti, R.M., Gonçalves, J.H. (Eds.), Geologia, Tectônica e Recursos Minerais do Brasil, vol. 5. Texto, mapas e SIG. CPRM-Serviço Geológico do Brasil, pp. 227–334.

Delor, C., Lahondère, D., Egal, E., Lafon, J.M., Cocherie, A., Guerrot, C., Rossi, P., Truffert, C., Théveniaut, H., Phillips, D., Avelar, V.G., 2003a. Transamazonian Crustal Growth and Reworking as Revealed by the 1:500,000-scale Geological Map of French Guiana, 2nd ed., Geol. France 2–4, 5–57.

Delor, C., Roever, E.W.F., Lafon, J.M., Lahondère, D., Rossi, P., Cocherie, A., Guerrot, C., Potrel, A., 2003b. The Bakhuis ultrahigh-temperature granulite belt (Suriname). II. Implications for late Transamazonian crustal stretching in a revised Guiana Shield framework. Geol. France 2–4, 207–230.

Endo, I., Machado, R., 2002. Reavaliação e novos dados geocronológicos (Pb/Pb e K/Ar) da região do Quadrilátero Ferrífero e adjacências. Geol. USP Série Científica 2, 23–40.

Faraco, M.T.L, Vale, A.G., Santos, J.O.S., Luzardo, R., Ferreira, A.L., Oliveira, M.A., Marinho, P.A.C., 2005. Levantamento Geológico da Região ao Norte da Província Carajás. In: Souza, V.S., Horbe, A.M.C. (Eds.), Contribuições a Geologia da Amazôn. 4, 32–44.

Fetter, A.H., Van Schmus, W.R., Santos, T.J.S., Nogueira Neto, J.A., Arthaud, M.H., 2000. U–Pb and Sm–Nd geochronological constraints on the crustal evolution and basement architecture of Ceará State, NW Borborema Province. NE Brazil: Implications for the existence of the Paleoproterozoic Supercontinent "Atlantica". Revista Brasil. Geociências 30 (1), 102–106.

Feybesse, J.L., Milési, J.P., 1994. The Archean/Paleoproterozoic contact zone in West Africa: a mountain belt of décollement thrusting and folding on a continental margin related to 2.1 Ga converence of Archean cratons? Precam. Res. 69., 199– 227.

Förster, H.-J., Tischendorf, G., Trumbull, R.B., 1997. An evaluation of Rb versus (Y + Nb) discriminantion diagram to infer tectonic setting of silicic igneous rocks. Lithos 40., 261–293.

Gaudette, H.E., Lafon, J.M., Macambira, M.J.B., Moura, C.A.V., Scheller, T., 1998. Comparison of single filament Pb evaporation/ionization zircon ages

with conventional U–Pb results: examples from the Precambrian of Brazil. J. South Am. Earth Sci. 11 (4), 351–363.

Harris, N.B., Pearce, J.A., Tindle, A.G., 1986. Geochemical characteristics of collision-zone magmatism. In: Coward, M.P., Ries, A.C. (Eds.), Collision Tectonics, vol. 19. Geological Society Special Publication, pp. 67–81.

Hartmann, L.A., Philipp, R.P., Liu, D., Wan, Y., Wang, Y., Santos, J.O.S., Vasconcellos, M.A.Z., 2004. Paleoproterozoic magmatic provenance of detrital zircons, Porongos Complex Quartzites, southern Brazilian Shield. Int. Geol. Rev. 46 (2), 127– 157.

Issler, R.S., Andrade, A.R.F., Montalvão, R.M.G., Guimarães, G., Silva, G.G., Lima, M.I.C., 1974. Geologia, Folha SA, 22, Belém, DNPM/Radam, v., 5, pp. 1–71.

Jorge João, X.S., Vale, A.G., Lobato, T.A.M., 1987. Programa Levantamentos Geológicos Básicos do Brasil. Altamira. Folha SA.22-Y-D. Estado do Pará. CPRM/DNPM, 31 pp.

Klein, E.L., Rosa-Costa, L.T., Lafon, J.M., 2003. Magmatismo Paleoarqueano (3.32 Ga) na região do Rio Cupixi, SE do Amapá, SE do Escudo das Guianas. Simpósio de Geologia da Amazônia, vol. 8, Sociedade Brasileira de Geologia, Manaus, Brazil, Resumos Expandidos, CD ROM.

Kober, B., 1986. Whole-grain evaporation for $^{207}Pb/^{206}Pb$-age investigations on single zircons using a double-filament thermal ion source. Contrib. Mineral. Petrol. 93, 482–490.

Kober, B., 1987. Single-zircon evaporation combined with Pb^{+} emitter bedding for $^{207}Pb/^{206}Pb$-age investigations using thermal ion mass spectrometry, and implications to zirconology. Contrib. Mineral. Petrol. 96, 63–71.

Lafon, J.M., Rossi, P., Delor, Barbosa, O.S., 2001. Granulitos tardi-transamazônicos (2.06 Ga) na região norte do Estado do Amapá: o charnoquito de Calçoene. Simpósio de Geologia da Amazônia, vol. 7, Sociedade Brasileira de Geologia, Belém, Brazil, Resumos Expandidos, CD ROM.

Lamarão, C.N., Dall'Agnol, R., Lafon, J.M., Lima, E.F., 2002. Geology, geochemistry, and Pb–Pb zircon geochronology of the Paleoproterozoic magmatism of Vila Riozinho, Tapajós Gold Province, Amazonian craton, Brazil. Precam. Res. 119, 189–223.

Ledru, P., Johan, V., Milési, J.P., Tegyey, M., 1994. Markers of the last stages of the Paleoproterozoic collision: evidence for a 2 Ga continent involving circum-South Atlantic provinces. Precam. Res. 69, 69–191.

Liégeois, J.P., 1998. Some words on the post-collisional magmatism—preface to special edition on post-collisional magmatism. Lithos, 45.

Liégeois, J.P., Navez, J., Hertogen, J., Black, R., 1998. Contrasting origin of post-collisional high-K calc-alkaline and shoshonitic versus alkaline and peralkaline granitoids. The use of sliding normalization. Lithos 45, 1–28.

Ludwig, K.R., 2001. Squid Version 1.03—A User's Manual, No. 2. Berkeley Geochronology Center Special Publication, 18 pp.

Ludwig, K.R., 2003. User's Manual for Isoplot/Ex version 3.00—A Geochronology Toolkit for Microsoft Excel, No. 4. Berkeley Geochronological Center Special Publication, 70 pp.

Macambira, M.J.B., Barros, C.E.M., Silva, D.C.C., Santos, M.C.C., 2001. Novos dados geológicos e geocronológicos para a região ao norte da Província de Carajás, evidências para o estabelecimento do limite Arqueano-Paleoproterozóico no sudeste do Cráton Amazônico. Simpósio de Geologia da Amazônia, vol. 7, Sociedade Brasileira de Geologia, Belém, Brazil, Resumos Expandidos, CD ROM.

Macambira, M.J.B., Silva, D.C.C., Barros, C.E.M., Scheller, T., 2003. New isotope evidences confirming the existence of a Paleoproterozoic terrain in the region at north of the Carajás Mineral Province. In: Proceedings of the South American Symposium on Isotope Geology, vol. 4, Salvador, Brazil, Short Papers, pp. 205–208.

Macambira, M.J.B., Silva, D.C.C., Vasquez, M.L., Barros, C.E.M., 2004. Investigação do limite Arqueano-Paleoproterozóico ao norte da Província de Carajás, Amazônia Oriental. Congresso Brasileiro de Geologia, vol. 42, Sociedade Brasileira de Geologia, Araxá, Brazil, Resumos, CD ROM.

Nomade, S., Féraud, G., Chen, Y., Pouclet, A., 2002. Thermal and tectonic evolution of the Paleoproterozoic Transamazonian orogen as deduced from $^{40}Ar/^{39}Ar$ and AMS along the Oyapok River (French Guiana). Precam. Res. 114, 35–53.

Oliveira, E.C., 2002. Implantação do método Sm–Nd em minerais metamórficos e sua aplicação em rochas da região central do Amapá, sudeste do Escudo das Guianas. MSc thesis, Universidade Federal do Pará, Belém, Brazil, 109 pp.

Oliveira, J.R., Silva Neto, C.S., Costa, E.J.S. 1994. Programa Levantamentos Geológicos Básicos do Brasil. Serra Pelada. Folha SB.22-X-C. Estado do Pará. CPRM, Serviço Geológico do Brasil, 220 pp.

Paces, J.B., Miller, J.D., 1993. Precise U–Pb ages of Duluth Complex and related mafic intrusions, northeastern Minnesota: geochronological insights into physical, petrogenetic, paleomagnetic and tectonomagmatic process associated with the 11 Ga midcontinental system. J. Geophys. Res. 98, 13997–14013.

Pearce, J.A., 1996. Source and setting of granitic rocks. Episodes 19, 120–125.

Pimentel, M.M., Spier, C.A., Ferreira Filho, C.F., 2002. Estudo Sm–Nd do Complexo Máfico-Ultramáfico Bacuri, Amapá: idade da intrusão, metamorfismo e natureza do magma original. Revista Brasil. Geociências 32, 371–376.

Plumb, K.A., 1991. New Precambrian time-scale. Episodes 14 (2), 139–140.

Ricci, P.S.F., 2006a. Mineralogically bizarre charnockitoids of the Bacajá High-Grade Block (Pará): discharnockitized and reemplaced plutons mistakenly confused with granitoids crystallized at shallower crustal levels. Simpósio de Geologia da Amazônia, vol. 9, Sociedade Brasileira de Geologia, Belém, Belém, Brazil, Resumos Expandidos, CD ROM.

Ricci, P.S.F., 2006b. Unprecedented recognition of jotunitic-mangeritic orogenic bodies from the low course of the Iriri River to Tucuruí Lake (Pará): implications for the Bacajá High-Grade Block boundaries. Simpósio de Geologia da Amazônia, vol. 9, Sociedade Brasileira de Geologia, Belém, Belém, Brazil, Resumos Expandidos, CD ROM.

Ricci, P.S.F., Carvalho, J.M.A., Rosa-Costa, L.T Lafon, J.M., 2002. Plúton charnoenderbítico Arqueano intrusivo nos ortognaisses granulíticos do Cinturão Jari – Terreno Arqueano expressivo do sudeste do Escudo das Guianas. Congresso Brasileiro de Geologia, vol. 41, Sociedade Brasileira de Geologia, João Pessoa, Brazil, Resumos, pp. 524.

Roever, E.W.F., Lafon, J.M., Delor, C., Cocherie, A., Rossi, P., Guerrot, C., Potrel, A., 2003. The Bakhuis ultrahigh-temperature granulite belt (Suriname). I. Petrological and geochronological evidence for a counterclockwise P–T path at 2.07–2.05 Ga. Géol. France 2–4, 175–206.

Rolando, A.P., Macambira, M.J.B., 2003. Archean crust formation in Inajá Range area, SSE of Amazonian Craton, Brazil, based on zircon ages and Nd isotopes. In: Proceedings of the South American Symposium on Isotope Geology, vol. 4, Salvador, Brazil, Short Papers, pp. 268–270.

Rosa-Costa, L.T., Lafon, J.M., Cocherrie, A., Delor, C., in press. Electron microprobe U-Th-Pb monazite dating deciphering the age of the high-grade metamorphic overprint on Archean rocks from southern Guiana Shield, north of Amazon Craton, Brazil. J. South Am. Earth Sci.

Rosa-Costa, L.T., Lafon, J.M., Delor, C., 2006. Zircon geochronology and Sm–Nd isotopic study: further constraints for the Archean and Paleoproterozoic geodynamic evolution of the southeastern Guiana Shield, north of Brazil. Gondwana Res. 10, 277–300.

Rosa-Costa, L.T, Ricci, P.S.F., Lafon, J.M., Vasquez, M.L., Carvalho, J.M.A., Klein, E.L., Macambira, E.M.B., 2003. Geology and geochronology of Archean and Paleoproterozoic domains of the southeastern Amapá and northwestern Pará, Brazil–southeastern Guiana Shield. Géol. France, 2–4, 101–120.

Santos, J.O.S., 2003. Geotectônica dos Escudos da Guiana e Brasil Central. In: Bizzi, L.A., Schobbenhaus, C., Vidotti, R.M., Gonçalves, J.H. (Eds.), Geologia, Tectônica e Recursos Minerais do Brasil. Texto, mapas e SIG. CPRM-Serviço Geológico do Brasil, vol. 4, pp. 169–226.

Santos, J.O.S., Hartmann, L.A., Bossi, J., Campal, N., Schipilov, A., Piñeyro, D., McNaughton, N.J., 2003a. Duration of the Trans-Amazonian Cycle and its correlation within South America Based on U–Pb SHRIMP Geochronology of the La Plata Craton, Uruguay. Int. Geol. Rev. 45, 27–48.

Santos, J.O.S., Hartmann, L.A., Faria, M.S.G., Riker, S.R., Souza, M.M., Almeida, M.E. McNaughton, N.J. 2006. A compartimentação do Cráton Amazonas em províncias: avanços ocorridos no período 2000–2006. Simpósio de Geologia da Amazônia, vol. 9, Sociedade Brasileira de Geologia, Belém, Brazil, Resumos Expandidos, CD ROM.

Santos, J.O.S., Hartmann, L.A., Gaudette, H.E, Groves, D.I., McNaughton, N.J, Flecher, I.R., 2000. New understanding of the Amazon Craton provinces, based on field mapping and U–Pb and Sm–Nd geochronology. Gondwana Res. 3 (4), 453–488.

Santos, J.O.S., Potter, P.E., Reis, N.J., Hartmann, L.A., Fletcher, I.R., McNaughton, N.J., 2003b. Age, source and regional stratigraphy of the Roraima Supergroup and Roraima-like outliers in northern South America based on U–Pb geochronology. Geol. Soc. Am. Bull. 115 (3), 331–348.

Santos, J.O.S., Van Breemen, O.B., Groves, D.I, Hartmann, L.A., Almeida, M.E., McNaughton, N.J., Fletcher, R.I, 2004. Timing and evolution of multiple Paleoproterozoic magmatic arcs in the Tapajós Domain, Amazon Craton: constraints from SHRIMP and TIMS zircon, baddeleyite and titanite U–Pb geochronology. Precam. Res. 13, 73–109.

Santos, M.V., Souza Filho, E.E., Tassinari, C.C.G., Teixeira, W., Ribeiro, A.C.O., Payolla, B.L, Vasconi, A.V., 1988. Litoestratigrafia das rochas pré-cambrianas na bacia do médio Rio Xingu–Altamira, PA. Congresso Latino-americano de Geologia, vol. 7, Sociedade Brasileira de Geologia, Belém, Brazil, Anais, 1, pp. 363–377.

Sato, K., Tassinari, C.C.G., 1997. Principais eventos de acreção continental no Cráton Amazônico baseados em idade-modelo Sm–Nd, calculada em evoluções de estágio único e estágio duplo. In: Costa, M.L.C., Angélica, R.S. (Eds.), Contribuição à Geologia da Amazônia, vol. 1. Sociedade Brasileira de Geologia, Belem, Brazil, pp. 91–142.

Schobbenhaus, C, Brito Neves, B.B. 2003. Geologia do Brasil no contexto da Plataforma Sul-Americana In: Bizzi, L.A., Schobbenhaus, C., Vidotti, R.M., Gonçalves, J.H. (Eds.), Geologia, Tectônica e Recursos Minerais do Brasil. Texto, mapas e SIG. CPRM-Serviço Geológico do Brasil, vol. 1, pp. 5–54.

Silva, G.G., Lima, M.I.C., Andrade, A.R.F., Issler, R.S., Guimarães, G., 1974. Geologia. Folha SB.22, Araguaia e parte da SC.22, Tocantins. DNPM/Radam, vol. 4, pp. 1–72.

Silva, L.C., Armstrong, R.A., Delgado, I.M., Pimentel, M.M., Arcanjo, J.B., Melo, R.C., Teixeira, L.R., Jost, H., Cardoso Filho, J.M., Pereira, L.H.M., 2002. Reavaliacão da evolucão geológica em terrenos Pré-cambrianos brasileiros com base em novos dados U–Pb SHRIMP Parte I: Limite centro-oriental do Cráton do São Francisco. Revista Brasil. Geociências 33 (4), 501–502.

Souza, V.S., Macambira, M.J.B., Koutchoubey, B., 2003. Idade de zircão do granito Felício Turvo, garimpo de ouro do Manelão, regão do Bacajá (PA): implicações tectônicas. Simpósio de Geologia da Amazônia, vol. 8, Sociedade Brasileira de Geologia, Manaus, Brazil, Resumos Expandidos, CD ROM.

Stacey, J.S., Kramers, J.D., 1975. Approximation of terrestrial lead isotopic evolution by a two stage model. Earth Planet. Sci. Lett. 26, 207–221.

Sylvester, P.J., 1989. Post-collisional alkaline granites. J. Geol. 97, 261–283.

Tassinari, C.C.G., Bettencourt, J.S., Geraldes, M.C., Macambira, M.J.B., Lafon, J.M., 2000. The Amazonian Craton. In: Cordani, U.G., Milani, E.J., Thomaz Filho, A., Campos, D.A. (Eds.), Tectonic Evolution of South America. Rio de Janeiro, Brazil, pp. 41–95.

Tassinari, C.C.G., Macambira, M.J.B., 1999. Geochronological provinces of the Amazonian Craton. Episodes 22, 174–182.

Tassinari, C.C.G., Macambira, M.J.B., 2004. A evolução tectônica do Cráton Amazônico. In: Mantesso-Neto, V., Bartorelli, A., Carneiro, C.D.R., Brito Neves, B.B. (Eds.), Geologia do Continente Sul-Americano: Evolução da Obra de Fernando Flávio Marques de Almeida. pp. 471–485.

Teixeira, W., Tassinari, C.C.G., Cordani, U.G., Kawashita, K., 1989. A review of the geochronology of the Amazonian Craton: tectonic implications. Precam. Res. 42, 213– 227.

Vanderhaeghe, O., Ledru, P., Thiéblemont, D., Egal, E., Cocherie, A., Tegyey, M., Milési, J.J., 1998. Contrasting mechanism of crustal growth geodynamic evolution of the Paleoproterozoic granite-greenstone belts of French Guyana. Precam. Res. 92, 165–193.

Vasquez, M.L., Klein, E.L., Ricci, P.S.F., 2002. Granitóides pós-colisionais da porção leste da Província Tapajós. In: Klein, E.L., Vasquez, M.L, Rosa-Costa, L.T. (Eds.), Contribuições à Geologia da Amazônia, vol. 3. Sociedade Brasileira de Geologia, Belém, Brazil, pp. 67–84.

Vasquez, M.L., Macambira, M.J.B., Galarza, M.A., 2005. Granitóides Transamazônicos da Região Iriri-Xingu Para, Novos dados geológicos e geocronológicos. In: Souza, V.S., Horbe, A.M.C. (Eds.), Contribuições à Geologia da Amazônia, Sociedade Brasileira de Geologia, vol. 4. Belem, Brazil, pp. 16–31.

Williams, I.S. 1998. U–Th–Pb geochronology by ion microprobe. In: McKibben, M.A., Shanks III, W.C., Rydley, W.I. (Eds.), Applications of Microanalytical Techniques to Understanding Mineralizing Processes, Rev. Econ. Geol. 7, 1–35 (Chapter 1).